Chapter 3

Nonlinear Pulse Propagation

There are many nonlinear pulse propagation problems worthwhile of being considered in detail, such as pulse propagation through a two-level medium in the coherent regime, which leads to self-induced transparency and solitons governed by the Sinus-Gordon-Equation. The basic model for the medium is the two-level atom discussed before with infinitely long relaxation times $T_{1,2}$, i.e. assuming that the pulses are much shorter than the dephasing time in the medium. In such a medium pulses exist, where the first half of the pulse fully inverts the medium and the second half of the pulse extracts the energy from the medium. The integral over the Rabi-frequency as defined in Eq.(2.39) is than a mutiple of 2π. The interested reader is refered to the book of Allen and Eberly [1]. Here, we are interested in the nonlinear dynamics due to the Kerr-effect which is most important for understanding pulse propagation problems in optical communications and short pulse generation.

3.1 The Optical Kerr-effect

In an isotropic and homogeneous medium, the refractive index can not depend on the direction of the electric field. Therefore, to lowest order, the refractive index of such a medium can only depend quadratically on the field, i.e. on the intensity [22]

$$n = n(\omega, |A|^2) \approx n_0(\omega) + n_{2,L}|A|^2. \tag{3.1}$$

Here, we assume, that the pulse envelope A is normalized such that $|A|^2$ is the intensity of the pulse. This is the optical Kerr effect and $n_{2,L}$ is called

Material	Refractive index n	$n_{2,L}[cm^2/W]$
Sapphire (Al_2O_3)	1.76 @ 850 nm	$3{\cdot}10^{-16}$
Fused Quarz	1.45 @ 1064 nm	$2.46{\cdot}10^{-16}$
Glass (LG-760)	1.5 @ 1064 nm	$2.9{\cdot}10^{-16}$
YAG ($Y_3Al_5O_{12}$)	1.82 @ 1064 nm	$6.2{\cdot}10^{-16}$
YLF ($LiYF_4$), n_e	1.47 @ 1047 nm	$1.72{\cdot}10^{-16}$
Si	3.3 @ 1550 nm	$4{\cdot}10^{-14}$

Table 3.1: Nonlinear refractive index coefficients for different materials. In the literature most often the electro-statitic unit system is in use. The conversion is $n_{2,L}[cm^2/W] = 4.19 \cdot 10^{-3} n_{2,L}[esu]/n_0$

the intensity dependent refractive index coefficient. Note, the nonlinear index depends on the polarization of the field and without going further into details, we assume that we treat a linearily polarized electric field. For most transparent materials the intensity dependent refractive index is positive.

3.2 Self-Phase Modulation (SPM)

In a purely one dimensional propagation problem, the intensity dependent refractive index imposes an additional self-phase shift on the pulse envelope during propagation, which is proportional to the instantaneous intensity of the pulse

$$\frac{\partial A(z,t)}{\partial z} = -jk_0 n_{2,L}|A(z,t)|^2 A(z,t) = -j\delta|A(z,t)|^2 A(z,t). \tag{3.2}$$

where $\delta = k_0 n_{2,L}$ is the self-phase modulation coefficient. Self-phase modulation (SPM) leads only to a phase shift in the time domain. Therefore, the intensity profile of the pulse does not change only the spectrum of the pulse changes, as discussed in the class on nonlinear optics. Figure (3.1) shows the spectrum of a Gaussian pulse subject to SPM during propagation (for $\delta = 2$ and normalized units). New frequency components are generated by the nonlinear process via four wave mixing (FWM). If we look at the phase of the pulse during propagation due to self-phase modulation, see Fig. 3.2 (a), we find, that the pulse redistributes its energy, such that the low frequency contributions are in the front of the pulse and the high frequencies in the back of the pulse, similar to the case of positive dispersion.

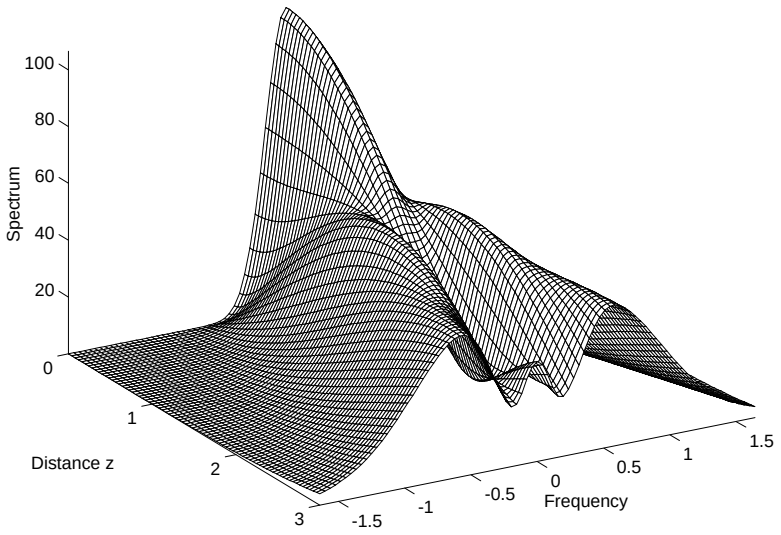

Figure 3.1: Spectrum $|\hat{A}(z, \omega = 2\pi f)|^2$ of a Gaussian pulse subject to self-phase modulation.

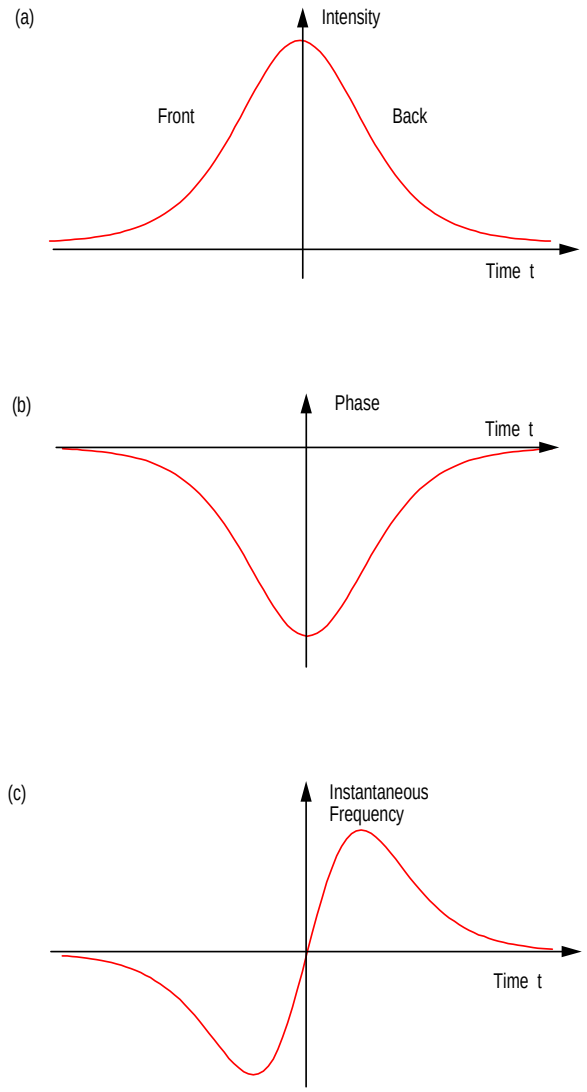

Figure 3.2: (a) Intensity, (b) phase and (c) instantaneous frequency of a Gaussian pulse during propagation through a medium with positive self-phase modulation.

3.3 The Nonlinear Schrödinger Equation

If both effects, dispersion and self-phase modulation, act simultaneously on the pulse, the field envelope obeys the equation

$$j\frac{\partial A(z,t)}{\partial z} = -D_2\frac{\partial^2 A}{\partial t^2} + \delta|A|^2 A, \tag{3.3}$$

This equation is called the Nonlinear Schrödinger Equation (NSE) - if we put the imaginary unit on the left hand side -, since it has the form of a Schrödinger Equation. Its called nonlinear, because the potential energy is derived from the square of the wave function itself. As we have seen from the discussion in the last sections, positive dispersion and positive self-phase modulation lead to a similar redistribution of the spectral components. This enhances the pulse spreading in time. However, if we have negative dispersion, i.e. a wave packet with high carrier frequency travels faster than a wave packet with a low carrier frequency, then, the high frequency wave packets generated by self-phase modulation in the front of the pulse have a chance to catch up with the pulse itself due to the negative dispersion. The opposite is the case for the low frequencies. This arrangement results in pulses that do not disperse any more, i.e. solitary waves. That negative dispersion is necessary to compensate the positive Kerr effect is also obvious from the NSE (3.3). Because, for a positive Kerr effect, the potential energy in the NSE is always negative. There are only bound solutions, i.e. bright solitary waves, if the kinetic energy term, i.e. the dispersion, has a negative sign, $D_2 < 0$.

3.3.1 The Solitons of the NSE

In the following, we study different solutions of the NSE for the case of negative dispersion and positive self-phase modulation. We do not intend to give a full overview over the solution manyfold of the NSE in its full mathematical depth here, because it is not necessary for the following. This can be found in detail elsewhere [4, 5, 6, 7].

Without loss of generality, by normalization of the field amplitude $A = \frac{A'}{\tau}\sqrt{\frac{2D_2}{\delta}}$, the propagation distance $z = z' \cdot \tau^2/D_2$, and the time $t = t' \cdot \tau$, the NSE (3.3) with negative dispersion can always be transformed into the

normalized form

$$j\frac{\partial A'(z',t)}{\partial z'} = \frac{\partial^2 A'}{\partial t'^2} + 2|A'|^2 A' \tag{3.4}$$

This is equivalent to set $D_2 = -1$ and $\delta = 2$. For the numerical simulations, which are shown in the next chapters, we simulate the normalized eq.(3.4) and the axes are in normalized units of position and time.

3.3.2 The Fundamental Soliton

We look for a stationary wave function of the NSE (3.3), such that its absolute square is a self-consistent potential. A potential of that kind is well known from Quantum Mechanics, the sech^2-Potential [8], and therefore the shape of the solitary pulse is a sech

$$A_s(z,t) = A_0 \text{sech}\left(\frac{t}{\tau}\right) e^{-j\theta}, \tag{3.5}$$

where θ is the nonlinear phase shift of the soliton

$$\theta = \frac{1}{2}\delta A_0^2 z \tag{3.6}$$

The soltion phase shift is constant over the pulse with respect to time in contrast to the case of self-phase modulation only, where the phase shift is proportional to the instantaneous power. The balance between the nonlinear effects and the linear effects requires that the nonlinear phase shift is equal to the dispersive spreading of the pulse

$$\theta = \frac{|D_2|}{\tau^2} z. \tag{3.7}$$

Since the field amplitude $A(z,t)$ is normalized, such that the absolute square is the intensity, the soliton energy fluence is given by

$$w = \int_{-\infty}^{\infty} |A_s(z,t)|^2 dt = 2A_0^2\tau. \tag{3.8}$$

From eqs.(3.6) to (3.8), we obtain for constant pulse energy fluence, that the width of the soliton is proportional to the amount of negative dispersion

$$\tau = \frac{4|D_2|}{\delta w}. \tag{3.9}$$

Note, the pulse area for a fundamental soliton is only determined by the dispersion and the self-phase modulation coefficient

$$\text{Pulse Area} = \int_{-\infty}^{\infty} |A_s(z,t)|dt = \pi A_0 \tau = \pi \sqrt{\frac{|D_2|}{2\delta}}. \tag{3.10}$$

Thus, an initial pulse with a different area can not just develope into a pure soliton.

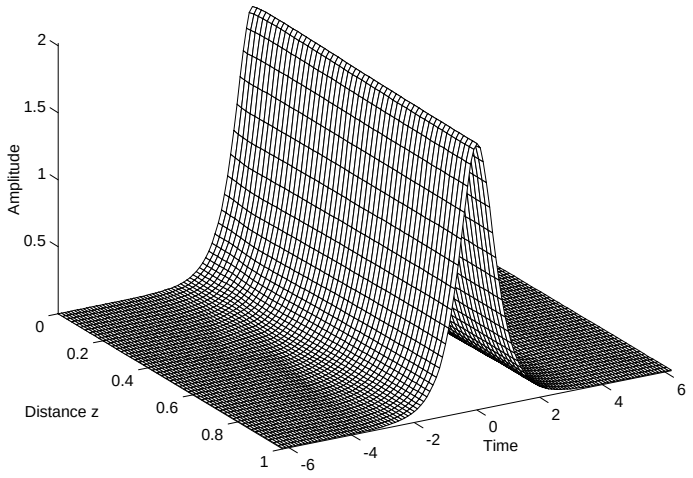

Figure 3.3: Propagation of a fundamental soliton.

Fig. 3.3 shows the numerical solution of the NSE for the fundamental soliton pulse. The distance, after which the soliton aquires a phase shift of $\pi/4$, is called the soliton period, for reasons, which will become clear in the next section.

Since the dispersion is constant over the frequency, i.e. the NSE has no higher order dispersion, the center frequency of the soliton can be chosen arbitrarily. However, due to the dispersion, the group velocities of the solitons with different carrier frequencies will be different. One easily finds by a Gallilei tranformation to a moving frame, that the NSE posseses the following general fundamental soliton solution

$$A_s(z,t) = A_0 \text{sech}(x(z,t))e^{-j\theta(z,t)}, \tag{3.11}$$

with

$$x = \frac{1}{\tau}(t - 2|D_2|p_0 z - t_0), \tag{3.12}$$

and a nonlinear phase shift

$$\theta = p_0(t - t_0) + |D_2| \left(\frac{1}{\tau^2} - p_0^2 \right) z + \theta_0. \tag{3.13}$$

Thus, the energy fluence w or amplitude A_0, the carrier frequency p_0, the phase θ_0 and the origin t_0, i.e. the timing of the fundamental soliton are not yet determined. Only the soliton area is fixed. The energy fluence and width are determined if one of them is specified, given a certain dispersion and SPM-coefficient.

3.3.3 Higher Order Solitons

The NSE has constant dispersion, in our case negative dispersion. That means the group velocity depends linearly on frequency. We assume, that two fundamental soltions are far apart from each other, so that they do not interact. Then this linear superpositon is for all practical purposes another solution of the NSE. If we choose the carrier frequency of the soliton, starting at a later time, higher than the one of the soliton in front, the later soliton will catch up with the leading soliton due to the negative dispersion and the pulses will collide.

Figure 3.4 shows this situation. Obviously, the two pulses recover completely from the collision, i.e. the NSE has true soliton solutions. The solitons have particle like properties. A solution, composed of several fundamental solitons, is called a higher order soliton. If we look closer to figure 3.4, we recognize, that the soliton at rest in the local time frame, and which follows the t = 0 line without the collision, is somewhat pushed forward due to the collision. A detailed analysis of the collision would also show, that the phases of the solitons have changed [4]. The phase changes due to soliton collisions are used to built all optical switches [10], using backfolded Mach-Zehnder interferometers, which can be realized in a self-stabilized way by Sagnac fiber loops.

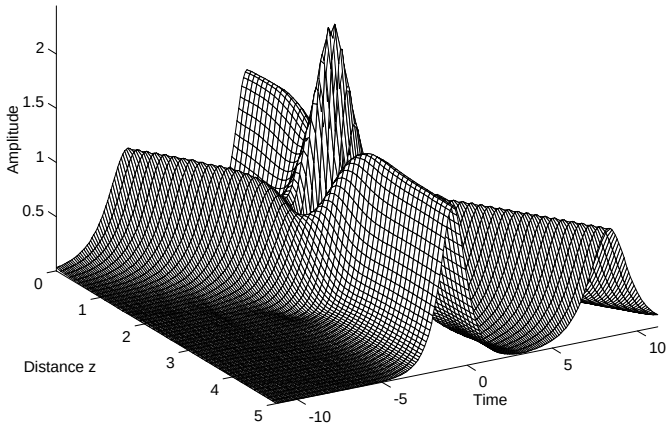

Figure 3.4: A soliton with high carrier frequency collides with a soliton of lower carrier frequency. After the collison both pulses recover completely.

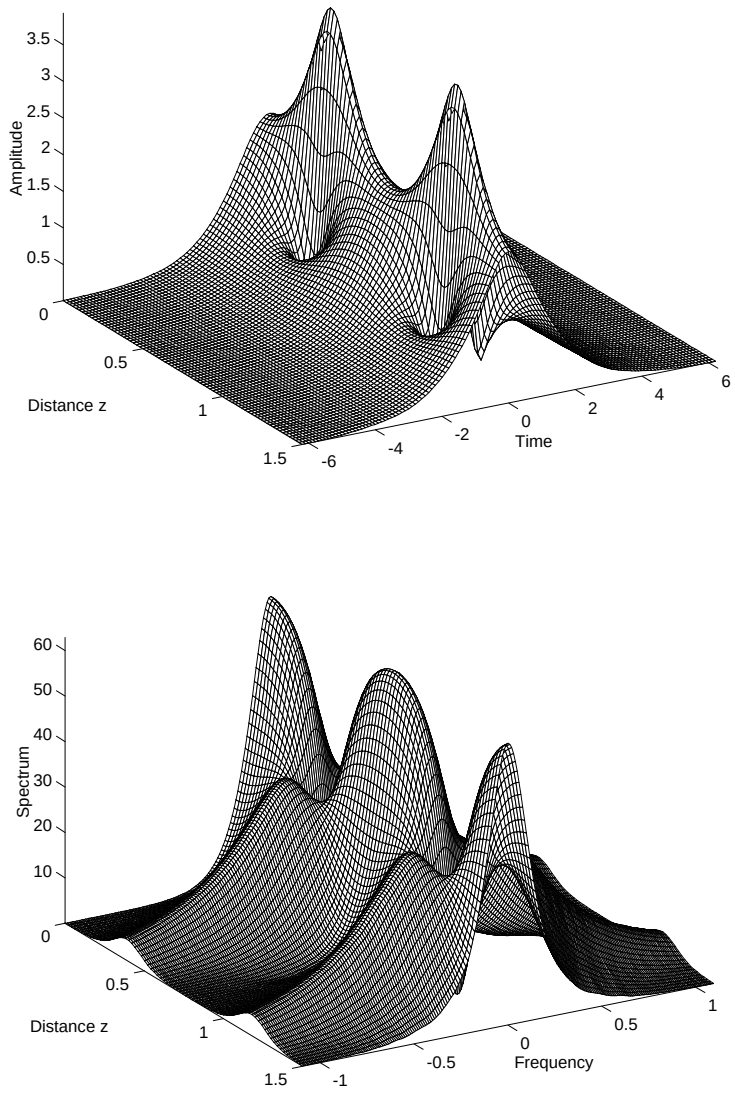

Figure 3.5: (a) Amplitude and, (b) Spectrum of a higher order soliton composed of two fundamental solitons with the same carrier frequency

The NSE also shows higher order soliton solutions, that travel at the same speed, i.e. they posses the same carrier frequency, the so called breather solutions. Figures 3.5(a) and (b) show the amplitude and spectrum of such a higher order soliton solution, which has twice the area of the fundamental soliton. The simulation starts with a sech-pulse, that has twice the area of the fundamental soliton, shown in figure 3.3. Due to the interaction of the two solitons, the temporal shape and the spectrum exhibits a complicated but periodic behaviour. This period is the soliton period $z = \pi/4$, as mentioned above. As can be seen from Figures 3.5(a) and 3.5(b), the higher order soliton dynamics leads to an enormous pulse shortening after half of the soliton period. This process has been used by Mollenauer, to build his soliton laser [11]. In the soliton laser, the pulse compression, that occures for a higher order soliton as shown in Fig. 3.5(a), is exploited for modelocking. Mollenauer pioneered soliton propagation in optical fibers, as proposed by Hasegawa and Tappert [3], with the soliton laser, which produced the first picosecond pulses at 1.55 μm. A detailed account on the soliton laser is given by Haus [12].

So far, we have discussed the pure soliton solutions of the NSE. But, what happens if one starts propagation with an input pulse that does not correspond to a fundamental or higher order soliton?

3.3.4 Inverse Scattering Theory

Obviously, the NSE has solutions, which are composed of fundamental solitons. Thus, the solutions obey a certain superposition principle which is absolutely surprising for a nonlinear system. Of course, not arbitrary superpositions are possible as in a linear system. The deeper reason for the solution manyfold of the NSE can be found by studying its physical and mathematical properties. The mathematical basis for an analytic formulation of the solutions to the NSE is the inverse scattering theory [13, 14, 4, 15]. It is a spectral tranform method for solving integrable, nonlinear wave equations, similar to the Fourier transform for the solution of linear wave equations [16].

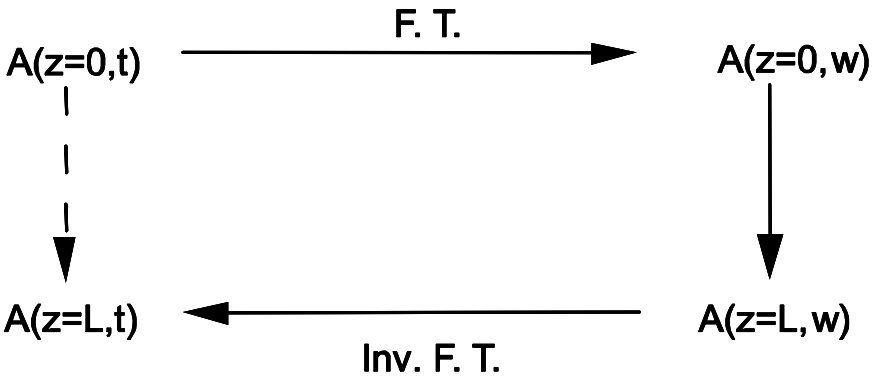

Figure 3.6: Fourier transform method for the solution of linear, time invariant partial differential equations.

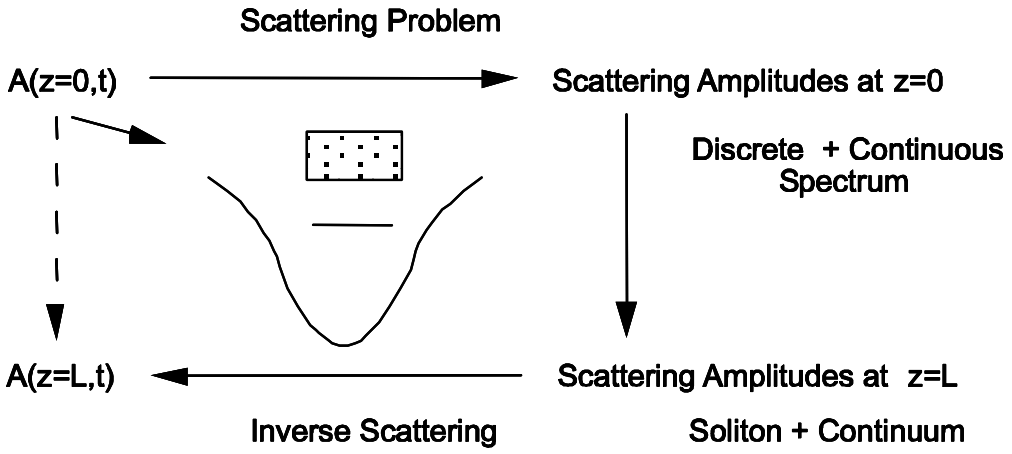

Figure 3.7: Schematic representation of the inverse scattering theory for the solution of integrable nonlinear partial differential equations.

Let's remember briefly, how to solve an initial value problem for a linear partial differential equation (p.d.e.), like eq.(2.184), that treats the case of a purely dispersive pulse propagation. The method is sketched in Fig. 3.6. We Fourier tranform the initial pulse into the spectral domain, because, the exponential functions are eigensolutions of the differential operators with

constant coefficients. The right side of (2.184) is only composed of powers of the differntial operator, therefore the exponentials are eigenfunctions of the complete right side. Thus, after Fourier transformation, the p.d.e. becomes a set of ordinary differential equations (o.d.e.), one for each partial wave. The excitation of each wave is given by the spectrum of the initial wave. The eigenvalues of the differential operator, that constitutes the right side of (2.184), is given by the dispersion relation, $k(\omega)$, up to the imaginary unit. The solution of the remaining o.d.e is then a simple exponential of the dispersion relation. Now, we have the spectrum of the propagated wave and by inverse Fourier transformation, i.e. we sum over all partial waves, we find the new temporal shape of the propagated pulse.

As in the case of the Fourier transform method for the solution of linear wave equations, the inverse scattering theory is again based on a spectral transform, (Fig.3.7). However, this transform depends now on the details of the wave equation and the initial conditions. This dependence leads to a modified superposition principle. As is shown in [7], one can formulate for many integrable nonlinear wave equations a related scattering problem like one does in Quantum Theory for the scattering of a particle at a potential well. However, the potential well is now determined by the solution of the wave equation. Thus, the initial potential is already given by the initial conditions. The stationary states of the scattering problem, which are the eigensolutions of the corresponding Hamiltonian, are the analog to the monochromatic complex oscillations, which are the eigenfunctions of the differential operator. The eigenvalues are the analog to the dispersion relation, and as in the case of the linear p.d.e's, the eigensolutions obey simple linear o.d.e's.

A given potential will have a certain number of bound states, that correspond to the discrete spectrum and a continuum of scattering states. The characteristic of the continuous eigenvalue spectrum is the reflection coefficient for waves scatterd upon reflection at the potential. Thus, a certain potential, i.e. a certain initial condition, has a certain discrete spectrum and continuum with a corresponding reflection coefficient. From inverse scattering theory for quantum mechanical and electromagnetic scattering problems, we know, that the potenial can be reconstructed from the scattering data, i.e. the reflection coefficient and the data for the discrete spectrum [**?**]. This is true for a very general class of scattering potentials. As one can almost guess now, the discrete eigenstates of the initial conditions will lead to soliton solutions. We have already studied the dynamics of some of these soliton so-

lutions above. The continuous spectrum will lead to a dispersive wave which is called the continuum. Thus, the most general solution of the NSE, for given arbitrary initial conditions, is a superposition of a soliton, maybe a higher order soliton, and a continuum contribution.

The continuum will disperse during propagation, so that only the soliton is recognized after a while. Thus, the continuum becomes an asympthotically small contribution to the solution of the NSE. Therefore, the dynamics of the continuum is completely discribed by the linear dispersion relation of the wave equation.

The back transformation from the spectral to the time domain is not as simple as in the case of the Fourier transform for linear p.d.e's. One has to solve a linear integral equation, the Marchenko equation [17]. Nevertheless, the solution of a nonlinear equation has been reduced to the solution of two linear problems, which is a tremendous success.

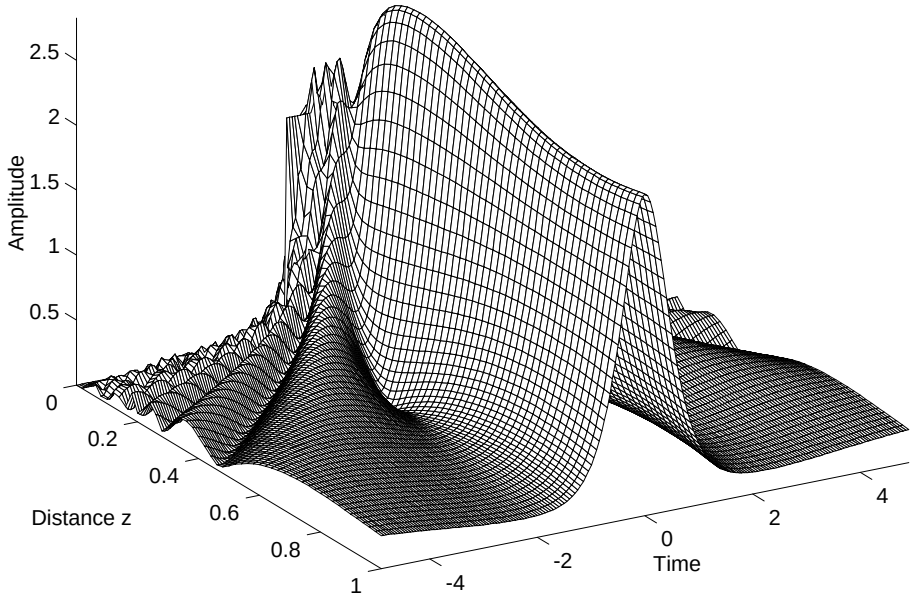

Figure 3.8: Solution of the NSE for an unchirped and rectangular shaped initial pulse.

To appreciate these properties of the solutions of the NSE, we solve the NSE for a rectangular shaped initial pulse. The result is shown in Fig. 3.8.

The scattering problem, that has to be solved for this initial condition, is the same as for a nonrelativistic particle in a rectangular potential box [32]. The depth of the potential is chosen small enough, so that it has only one bound state. Thus, we start with a wave composed of a fundamental soliton and continuum. It is easy to recognize the continuum contribution, i.e. the dispersive wave, that separates from the soliton during propagation. This solution illustrates, that soliton pulse shaping due to the presence of dispersion and self-phase modulation may have a strong impact on pulse generation [18]. When the dispersion and self-phase modulation are properly adjusted, soliton formation can lead to very clean, stable, and extremly short pulses in a modelocked laser.

3.4 Universality of the NSE

Above, we derived the NSE in detail for the case of disperison and self-phase modulation. The input for the NSE is surprisingly low, we only have to admitt the first nontrivial dispersive effect and the lowest order nonlinear effect that is possible in an isotropic and homogeneous medium like glass, gas or plasmas. Therefore, the NSE and its properties are important for many other effects like self-focusing [19], Langmuir waves in plasma physics, and waves in proteine molecules [20]. Self-focusing will be treated in more detail later, because it is the basis for Kerr-Lens Mode Locking.

3.5 Soliton Perturbation Theory

From the previous discussion, we have full knowledge about the possible solutions of the NSE that describes a special Hamiltonian system. However, the NSE hardly describes a real physical system such as, for example, a real optical fiber in all its aspects [21, 22]. Indeed the NSE itself, as we have seen during the derivation in the previous sections, is only an approximation to the complete wave equation. We approximated the dispersion relation by a parabola at the assumed carrier frequency of the soliton. Also the instantaneous Kerr effect described by an intensity dependent refractive index is only an approximation to the real $\chi^{(3)}$-nonlinearity of a Kerr-medium [23,

24]. Therefore, it is most important to study what happens to a soliton solution of the NSE due to perturbing effects like higher order dispersion, finite response times of the nonlinearites, gain and the finite gain bandwidth of amplifiers, that compensate for the inevitable loss in a real system.

The investigation of solitons under perturbations is as old as the solitons itself. Many authors treat the perturbing effects in the scattering domain [25, 26]. Only recently, a perturbation theory on the basis of the linearized NSE has been developed, which is much more illustrative then a formulation in the scattering amplitudes. This was first used by Haus [27] and rigorously formulated by Kaup [28]. In this section, we will present this approach as far as it is indispensible for the following.

A system, where the most important physical processes are dispersion and self-phase modulation, is described by the NSE complimented with some perturbation term F

$$\frac{\partial A(z,t)}{\partial z} = -j\left[|D_2|\frac{\partial^2 A}{\partial t^2} + \delta|A|^2 A\right] + F(A, A^*, z). \tag{3.14}$$

In the following, we are interested what happens to a solution of the full equation (3.14) which is very close to a fundamental soliton, i.e.

$$A(z,t) = \left[a(\frac{t}{\tau}) + \Delta A(z,t)\right] e^{-jk_s z}. \tag{3.15}$$

Here, $a(x)$ is the fundamental soliton according to eq.(3.5)

$$a(\frac{t}{\tau}) = A_0 \,\mathrm{sech}(\frac{t}{\tau}), \tag{3.16}$$

and

$$k_s = \frac{1}{2}\delta A_0^2 \tag{3.17}$$

is the phase shift of the soliton per unit length, i.e. the soltion wave vector.

A deviation from the ideal soliton can arise either due to the additional driving term F on the right side or due to a deviation already present in the initial condition. We use the form (3.15) as an ansatz to solve the NSE to first order in the perturbation ΔA, i.e. we linearize the NSE around the fundamental soliton and obtain for the perturbation

$$\begin{aligned}\frac{\partial \Delta A}{\partial z} &= -jk_s\left[\left(\frac{\partial^2}{\partial x^2} - 1\right)\Delta A + 2\mathrm{sech}^2(x)\left(2\Delta A + \Delta A^*\right)\right] \\ &\quad + F(A, A^*, z)e^{jk_s z},\end{aligned} \tag{3.18}$$

where $x = t/\tau$. Due to the nonlinearity, the field is coupled to its complex conjugate. Thus, eq.(3.18) corresponds actually to two equations, one for the amplitude and one for its complex conjugate. Therefore, we introduce the vector notation

$$\mathbf{\Delta A} = \begin{pmatrix} \Delta A \\ \Delta A^* \end{pmatrix}. \tag{3.19}$$

We further introduce the normalized propagation distance $z' = k_s z$ and the normalized time $x = t/\tau$. The linearized perturbed NSE is then given by

$$\frac{\partial}{\partial z'}\mathbf{\Delta A} = \mathbf{L}\mathbf{\Delta A} + \frac{1}{k_s}\mathbf{F}(A, A^*, z)e^{jz'} \tag{3.20}$$

Here, $\mathbf{L}$ is the operator which arises from the linearization of the NSE

$$\mathbf{L} = -j\boldsymbol{\sigma}_3 \left[(\frac{\partial^2}{\partial x^2} - 1) + 2\,\mathrm{sech}^2(x)(2 + \boldsymbol{\sigma}_1) \right], \tag{3.21}$$

where $\boldsymbol{\sigma}_i, i = 1, 2, 3$ are the Pauli matrices. For a solution of the inhomogeneous equation (3.20), we need the eigenfunctions and the spectrum of the differential operator $\mathbf{L}$. We found in section 3.3.2, that the fundamental soliton has four degrees of freedom, four free parameters. This gives already four known eigensolutions and mainsolutions of the linearized NSE, respectively. They are determined by the derivatives of the general fundamental soliton solutions according to eqs.(3.11) to (3.13) with respect to free parameters. These eigenfunctions are

$$\mathbf{f}_w(x) = \frac{1}{w}(1 - x\tanh x)a(x)\begin{pmatrix} 1 \\ 1 \end{pmatrix}, \tag{3.22}$$

$$\mathbf{f}_\theta(x) = -ja(x)\begin{pmatrix} 1 \\ -1 \end{pmatrix}, \tag{3.23}$$

$$\mathbf{f}_p(x) = -j\,x\tau a(x)\begin{pmatrix} 1 \\ -1 \end{pmatrix}, \tag{3.24}$$

$$\mathbf{f}_t(x) = \frac{1}{\tau}\tanh(x)\,a(x)\begin{pmatrix} 1 \\ 1 \end{pmatrix}, \tag{3.25}$$

and they describe perturbations of the soliton energy, phase, carrier frequency and timing. One component of each of these vector functions is shown in Fig. 3.9.

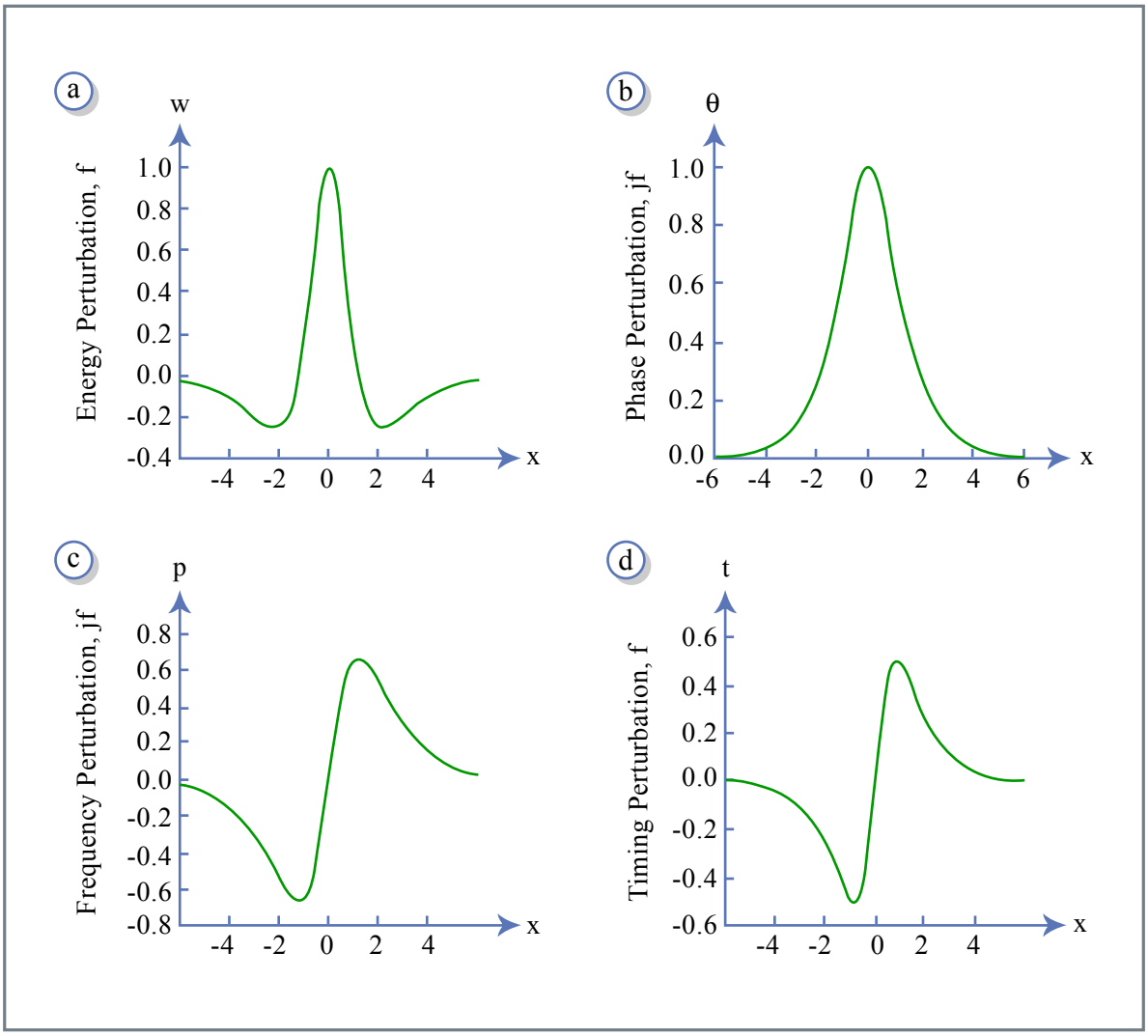

Figure 3.9: Perturabations in soliton amplitude (a), phase (b), frequency (c), and timing (d).

Figure by MIT OCW.

The action of the evolution operator of the linearized NSE on these soliton perturbations is

$$\mathbf{L}\mathbf{f}_w = \frac{1}{w}\mathbf{f}_\theta, \tag{3.26}$$

$$\mathbf{L}\mathbf{f}_\theta = 0, \tag{3.27}$$

$$\mathbf{L}\mathbf{f}_p = -2\tau^2\mathbf{f}_t, \tag{3.28}$$

$$\mathbf{L}\mathbf{f}_t = 0. \tag{3.29}$$

Equations (3.26) and (3.28) indicate, that perturbations in energy and carrier frequency are converted to additional phase and timing fluctuations of the pulse due to SPM and GVD. This is the base for soliton squeezing in optical fibers [27]. The timing and phase perturbations can increase without bounds, because the system is autonomous, the origin for the Gordon-Haus effect, [29] and there is no phase reference in the system. The full continuous spectrum of the linearized NSE has been studied by Kaup [28] and is given by

$$\mathbf{L}\mathbf{f}_k = \lambda_k \mathbf{f}_k, \tag{3.30}$$

$$\lambda_k = j(k^2+1), \tag{3.31}$$

$$\mathbf{f}_k(x) = e^{-jkx} \begin{pmatrix} (k - j\tanh x)^2 \\ \operatorname{sech}^2 x \end{pmatrix}, \tag{3.32}$$

and

$$\mathbf{L}\bar{\mathbf{f}}_k = \bar{\lambda}_k \bar{\mathbf{f}}_k, \tag{3.33}$$

$$\bar{\lambda}_k = -j(k^2+1), \tag{3.34}$$

$$\bar{\mathbf{f}}_k = \sigma_1 \mathbf{f}_k. \tag{3.35}$$

Our definition of the eigenfunctions is slightly different from Kaup [28], because we also define the inner product in the complex space as

$$< \mathbf{u}|\mathbf{v} >= \frac{1}{2}\int_{-\infty}^{+\infty} \mathbf{u}^+(x)\mathbf{v}(x)dx. \tag{3.36}$$

Adopting this definition, the inner product of a vector with itself in the subspace where the second component is the complex conjugate of the first component is the energy of the signal, a physical quantity.

The operator $\mathbf{L}$ is not self-adjoint with respect to this inner product. The physical origin for this mathematical property is, that the linearized system does not conserve energy due to the parametric pumping by the soliton. However, from (3.21) and (3.36), we can easily see that the adjoint operator is given by

$$\mathbf{L}^+ = -\sigma_3 \mathbf{L} \sigma_3, \tag{3.37}$$

and therefore, we obtain for the spectrum of the adjoint operator

$$\mathbf{L}^+ \mathbf{f}_k^{(+)} = \lambda_k^{(+)} \mathbf{f}_k^{(+)}, \tag{3.38}$$

$$\lambda_k^{(+)} = -j\,(k^2+1), \tag{3.39}$$

$$\mathbf{f}_k^{(+)} = \frac{1}{\pi(k^2+1)^2}\sigma_3 \mathbf{f}_k, \tag{3.40}$$

and

$$\mathbf{L}^{+}\bar{\mathbf{f}}_k^{(+)} = \bar{\lambda}_k^{(+)}\bar{\mathbf{f}}_k^{(+)}, \tag{3.41}$$

$$\bar{\lambda}_k^{(+)} = j(k^2+1), \tag{3.42}$$

$$\bar{\mathbf{f}}_k^{(+)} = \frac{1}{\pi(k^2+1)^2}\sigma_3\bar{\mathbf{f}}_k. \tag{3.43}$$

The eigenfunctions to $\mathbf{L}$ and its adjoint are mutually orthogonal to each other, and they are already properly normalized

$$\begin{aligned} < \mathbf{f}_k^{(+)}|\mathbf{f}_{k'} > &= \delta(k-k'), \qquad < \bar{\mathbf{f}}_k^{(+)}|\bar{\mathbf{f}}_{k'} >= \delta(k-k') \\ < \bar{\mathbf{f}}_k^{(+)}|\mathbf{f}_{k'} > &= < \mathbf{f}_k^{(+)}|\bar{\mathbf{f}}_{k'} >= 0. \end{aligned}$$

This system, which describes the continuum excitations, is made complete by taking also into account the perturbations of the four degrees of freedom of the soliton (3.22) - (3.25) and their adjoints

$$\mathbf{f}_w^{(+)}(x) = j2\tau\sigma_3\mathbf{f}_\theta(x) = 2\tau a(x)\begin{pmatrix} 1 \\ 1 \end{pmatrix}, \tag{3.44}$$

$$\begin{aligned} \mathbf{f}_\theta^{(+)}(x) &= -2j\tau\sigma_3\mathbf{f}_w(x) \\ &= \frac{-2j\tau}{w}(1 - x\tanh x)a(x)\begin{pmatrix} 1 \\ -1 \end{pmatrix}, \end{aligned} \tag{3.45}$$

$$\mathbf{f}_p^{(+)}(x) = -\frac{2j\tau}{w}\sigma_3\mathbf{f}_t(x) = \frac{2i}{w}\tanh x a(x)\begin{pmatrix} 1 \\ -1 \end{pmatrix}, \tag{3.46}$$

$$\mathbf{f}_t^{(+)}(x) = \frac{2j\tau}{w}\sigma_3\mathbf{f}_p(x) = \frac{2\tau^2}{w}xa(x)\begin{pmatrix} 1 \\ 1 \end{pmatrix}.. \tag{3.47}$$

Now, the unity can be decomposed into two projections, one onto the continuum and one onto the perturbation of the soliton variables [28]

$$\begin{aligned} \delta(x-x') &= \int_{-\infty}^{\infty} dk \left[|\mathbf{f}_k >< \mathbf{f}_k^{(+)}| + |\bar{\mathbf{f}}_k >< \bar{\mathbf{f}}_k^{(+)}|\right] \\ &+ |\mathbf{f}_w >< \mathbf{f}_w^{(+)}| + |\mathbf{f}_\theta >< \mathbf{f}_\theta^{(+)}| \\ &+ |\mathbf{f}_p >< \mathbf{f}_p^{(+)}| + |\mathbf{f}_t >< \mathbf{f}_t^{(+)}|. \end{aligned} \tag{3.48}$$

Any deviation ΔA can be decomposed into a contribution that leads to a soliton with a shift in the four soliton paramters and a continuum contribution a_c

$$\mathbf{\Delta A}(z') = \Delta w(z')\mathbf{f}_w + \Delta\theta(z')\mathbf{f}_\theta + \Delta p(z')\mathbf{f}_p + \Delta t(z')\mathbf{f}_t + \mathbf{a}_c(z'). \tag{3.49}$$

Further, the continuum can be written as

$$\mathbf{a}_c = \int_{-\infty}^{\infty} dk \left[g(k)\mathbf{f}_k(x) + \bar{g}(k)\bar{\mathbf{f}}_k(x) \right]. \tag{3.50}$$

If we put the decomposition (3.49) into (3.20) we obtain

$$\begin{aligned} &\frac{\partial \Delta w}{\partial z'}\mathbf{f}_w + \frac{\partial \Delta\theta}{\partial z'}\mathbf{f}_\theta + \frac{\partial \Delta p}{\partial z'}\mathbf{f}_p + \frac{\partial \Delta t}{\partial z'}\mathbf{f}_t + \frac{\partial}{\partial z'}\mathbf{a}_c = \\ &\mathbf{L}\left(\Delta w(z')\mathbf{f}_w + \Delta p(z')\mathbf{f}_p + \mathbf{a}(z')_c\right) + \frac{1}{k_s}\mathbf{F}(A, A^*, z')e^{-iz'}. \end{aligned} \tag{3.51}$$

By building the scalar products (3.36) of this equation with the eigensolutions of the adjoint evolution operator (3.38) to (3.43) and using the eigenvalues (3.26) to (3.35), we find

$$\frac{\partial}{\partial z'}\Delta w = \frac{1}{k_s} < \mathbf{f}_w^{(+)} | \mathbf{F} e^{jz'} >, \tag{3.52}$$

$$\frac{\partial}{\partial z'}\Delta\theta = \frac{\Delta W}{W} + \frac{1}{k_s} \mathbf{f}_\theta^{(+)} | \mathbf{F} e^{jz'} >, \tag{3.53}$$

$$\frac{\partial}{\partial z'}\Delta p = \frac{1}{k_s} < \mathbf{f}_p^{(+)} | \mathbf{F} e^{jz'} >, \tag{3.54}$$

$$\frac{\partial}{\partial z'}\Delta t = 2\tau\Delta p + \frac{1}{k_s} < \mathbf{f}_t^{(+)} | \mathbf{F} e^{jz'} >, \tag{3.55}$$

$$\frac{\partial}{\partial z'} g(k) = j(1+k^2)g(k) + \frac{1}{k_s} < \mathbf{f}_k^{(+)} \mathbf{F}(A, A^*, z') e^{jz'} > . \tag{3.56}$$

Note, that the continuum $\mathbf{a}_c$ has to be in the subspace defined by

$$\sigma_1 \mathbf{a}_c = \mathbf{a}_c^*. \tag{3.57}$$

The spectra of the continuum $g(k)$ and $\bar{g}(k)$ are related by

$$\bar{g}(k) = g(-k)^*. \tag{3.58}$$

Then, we can directly compute the continuum from its spectrum using (3.32), (3.50) and (3.57)

$$a_c = -\frac{\partial^2 G(x)}{\partial x^2} + 2\tanh(x)\frac{\partial G(x)}{\partial x} - \tanh^2(x)\, G(x) + G^*(x)\mathrm{sech}^2(x), \tag{3.59}$$

where $G(x)$ is, up to the phase factor $e^{iz'}$, Gordon's associated function [33]. It is the inverse Fourier transform of the spectrum

$$G(x) = \int_{-\infty}^{\infty} g(k)\, e^{ikx} dk. \tag{3.60}$$

Since $g(k)$ obeys eq.(3.56), Gordon's associated function obeys a pure dispersive equation in the absence of a driving term F

$$\frac{\partial G(z', x)}{\partial z'} = -j \left(1 + \frac{\partial^2}{\partial x^2}\right) G(z', x). \tag{3.61}$$

It is instructive to look at the spectrum of the continuum when only one continuum mode with normalized frequency k_0 is present, i.e. $g(k) = \delta(k - k_0)$. Then according to eqs. (3.59) and (3.60) we have

$$a_{c,k}(x) = \left[k_0^2 - 2jk_0 \tanh(x) - 1\right] e^{-jk_0 x} + 2\mathrm{sech}^2(x)\cos(x). \tag{3.62}$$

The spectrum of this continuum contribution is

$$\begin{aligned} \tilde{a}_{c,k}(\omega) &= 2\pi(k_0^2 - 1)\delta(\omega - k_0) + 2k_0\, P.V. \left(\frac{2}{\omega - k_0} + \frac{\pi}{\sinh\left(\frac{\pi}{2}(\omega - k_0)\right)}\right) \\ &+ \pi \frac{\omega - k_0}{\sinh\left(\frac{\pi}{2}(\omega - k_0)\right)} + \pi \frac{\omega + k_0}{\sinh\left(\frac{\pi}{2}(\omega + k_0)\right)}. \end{aligned} \tag{3.63}$$

3.6 Soliton Instabilities by Periodic Perturbations

Periodic perturbations of solitons are important for understanding ultrashort pulse lasers as well as ong distance optical communication systems [30, 31]. Along a long distance transmission system, the pulses have to be periodically amplified. In a mode-locked laser system, most often the nonlinearity, dispersion and gain occur in a lumped manner. The solitons propagating in these systems are only average solitons, which propagate through discrete components in a periodic fashion, as we will see later.

The effect of this periodic perturbations can be modelled by an additional term F in the perturbed NSE according to Eq.(3.14)

$$F(A, A^*, z) = j\xi \sum_{n=-\infty}^{\infty} \delta(z - nz_A) A(z, t). \tag{3.64}$$

The periodic kicking of the soliton leads to shedding of energy into continuum modes according to Eq.(3.56)

$$\frac{\partial}{\partial z}g(k) = jk_s(1+k^2)g(k) + < \mathbf{f}_k^{(+)}\mathbf{F}(A, A^*, z)e^{jk_s z} > . \tag{3.65}$$

$$\begin{aligned} < \quad & \mathbf{f}_k^{(+)}\mathbf{F}(A, A^*, z)e^{jk_s z} >= j\xi \sum_{n=-\infty}^{\infty} \delta(z - nz_A)\frac{1}{2} \cdot \qquad (3.66) \\ & \int_{-\infty}^{+\infty} \frac{1}{\pi(k^2+1)^2} e^{jkx} \begin{pmatrix} (k + j\tanh x)^2 \\ -\mathrm{sech}^2 x \end{pmatrix} \cdot \begin{pmatrix} 1 \\ 1 \end{pmatrix} A_0 \ \mathrm{sech}x \ dx \\ = \quad & j\xi \sum_{n=-\infty}^{\infty} \delta(z - nz_A) \cdot \qquad (3.67) \\ & \int_{-\infty}^{+\infty} \frac{A_0}{2\pi(k^2+1)^2} e^{jkx} \left(k^2 + 2jk\tanh x - 1\right) \cdot \mathrm{sech}x \ dx \end{aligned}$$

Note, $\frac{d}{dx}\mathrm{sech}x = -\mathrm{sech}x \tanh x$, and therefore

$$\begin{aligned} < \quad & \mathbf{f}_k^{(+)}\mathbf{F}(A, A^*, z)e^{jz} >= -j\xi \sum_{n=-\infty}^{\infty} \delta(z - nz_A) \cdot \\ & \int_{-\infty}^{+\infty} \frac{A_0}{2\pi(k^2+1)} e^{jkx} \cdot \mathrm{sech}x dx \\ = \quad & -j\xi \sum_{n=-\infty}^{\infty} \delta(z - nz_A) \frac{A_0}{4(k^2+1)} \ \mathrm{sech}\left(\frac{\pi k}{2}\right). \qquad (3.68) \end{aligned}$$

Using $\sum_{n=-\infty}^{\infty} \delta(z - nz_A) = \frac{1}{z_A} \sum_{m=-\infty}^{\infty} e^{jm\frac{2\pi}{z_A}z}$ we obtain

$$\frac{\partial}{\partial z}g(k) = jk_s(1+k^2)g(k) - j\frac{\xi}{z_A} \sum_{m=-\infty}^{\infty} e^{jm\frac{2\pi}{z_A}z} \frac{A_0}{4(k^2+1)} \ \mathrm{sech}\left(\frac{\pi k}{2}\right). \tag{3.69}$$

Eq.(3.69) is a linear differential equation with constant coefficients for the continuum amplitudes $g(k)$, which can be solved by variation of constants with the ansatz

$$g(k, z) = C(k, z)e^{jk_s(1+k^2)z}, \tag{3.70}$$

and initial conditions $C(z=0)=0$, we obtain

$$\frac{\partial}{\partial z}C(k,z) = -j\frac{\xi}{z_A}\sum_{m=-\infty}^{\infty}\frac{A_0}{4(k^2+1)}\,\mathrm{sech}\left(\frac{\pi k}{2}\right)e^{-j\left(k_s(1+k^2)-m\frac{2\pi}{z_A}z\right)}, \quad (3.71)$$

or

$$\begin{aligned} C(k,z) &= -j\frac{\xi}{z_A}\frac{A_0}{4(k^2+1)}\mathrm{sech}\left(\frac{\pi k}{2}\right)\cdot\sum_{m=-\infty}^{\infty}\int_0^z e^{j(-k_s(1+k^2)+m\frac{2\pi}{z_A})z}dz \\ &= -j\frac{\xi}{z_A}\frac{A_0}{4(k^2+1)}\mathrm{sech}\left(\frac{\pi k}{2}\right)\cdot \quad (3.72) \\ &\quad \sum_{m=-\infty}^{\infty}\frac{e^{j(-k_s(1+k^2)+m\frac{2\pi}{z_A})z}-1}{m\frac{2\pi}{z_A}-k_s(1+k^2)}. \end{aligned}$$

There is a resonant denominator, which blows up at certain normalized frequencies k_m for $z\to\infty$ Those frequencies are given by

$$m\frac{2\pi}{z_A}-k_s(1+k_m^2) = 0 \quad (3.73)$$

$$\text{or} \qquad k_m = \pm\sqrt{\frac{m\frac{2\pi}{z_A}}{k_s}-1}. \quad (3.74)$$

Removing the normalization by setting $k=\omega\tau$, $k_s=|D_2|/\tau^2$ and introducing the nonlinear phase shift of the soliton acquired over one periode of the perturbation $\phi_0=k_s z_A$, we obtain a handy formula for the location of the resonant sidebands

$$\omega_m = \pm\frac{1}{\tau}\sqrt{\frac{2m\pi}{\phi_0}-1}, \quad (3.75)$$

and the coefficients

$$\begin{aligned} C(\omega,z) &= -j\frac{\xi}{z_A}\frac{A_0}{4((\omega\tau)^2+1)}\mathrm{sech}\left(\frac{\pi\omega\tau}{2}\right) \quad (3.76) \\ &\quad \cdot\sum_{m=-\infty}^{\infty} z_A\frac{e^{j(-k_s(1+(\omega\tau)^2)+m\frac{2\pi}{z_A})z}-1}{2\pi m-\phi_0(1+(\omega\tau)^2)}. \end{aligned}$$

The coefficients stay bounded for frequencies not equal to the resonant condition and they grow linearly with z_A, at resonance, which leads to a destruction of the pulse. To stabilize the soliton against this growth of resonant

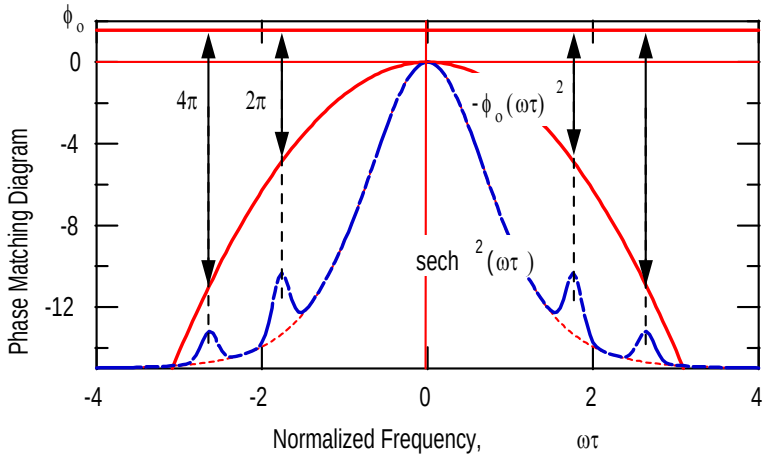

Figure 3.10: Phasematching between soliton and continuum due to periodic perturbations leads to resonant sideband generation. The case shown is for $\phi_0 = \pi/2$.

sidebands, the resonant frequencies have to stay outside the spectrum of the soliton, see Fig. 3.10, which feeds the continuum, i.e. $\omega_m \gg \frac{1}{\tau}$. This condition is only fulfilled if $\phi_0 \ll \pi/4$. This condition requires that the soliton period is much longer than the periode of the perturbation. As an example Fig. 3.10 shows the resonant sidebands observed in a fiber laser. For optical communication systems this condition requires that the soliton energy has to be kept small enough, so that the soliton periode is much longer than the distance between amplifiers, which constitute periodic perturbations to the soliton.These sidebands are often called Kelly-Sidebands, according to the person who first described its origin properly [30].

To illustrate its importance we discuss the spectrum observed from the longcavity Ti:sapphire laser system illustrated in Figure 3.11 and described in full detail in [37]. Due to the low repetitionrate, a rather large pulse energy builts up in the cavity, which leads to a large nonlinear phase shift per roundtrip.Figure 3.12 shows the spectrum of the output from the laser. The Kelly sidebands are clearly visible. It is this kind of instability, which limits further increase in pulse energy from these systems operating in the soliton pulse shaping regime. Energy is drained from the main pulse into the sidebands, which grow at the expense of the pulse. At some point the

Figure 3.11: Schematic layout of a high pulse energy laser cavity. All shaded mirrors are (Double-chirped mirrors) DCMs. The standard 100 MHz cavity with arms of 45 cm and 95 cm extends from the OC to M6 for the short and long arms respectively. The multiple pass cavity (MPC) is enclosed in the dotted box. The pump source is a frequency doubled Nd:Vanadate that produces up to 10W at 532 nm [37].

pulse shaping becomes unstable because of conditions to be discussed in later chapters.

Figure 3.12: Measured modelocked spectrum with a 16.5 nm FWHM centered at 788 nm

3.7 Pulse Compression

So far we have discussed propagation of a pulse in negative dispersive media and positive self-phase modulation. Then at large enough pulse energy a soliton can form, because the low and high frequency components generated by SPM in the front and the back of the pulse are slow and fast and therefore catch up with the pulse and stay together. What happens if the dispersion is positive? Clearly, the low and high frequency components generated by SPM in the front and back of the pulse are fast and slow and move away from the pulse in a continuous fashion. This leads to highly but linearly chirped pulse, which can be compressed after the nonlinear propagation by sending it through a linear negative dispersive medium or prism pair or grating pair. In that way, pulses can be compressed by large factors of 3 to 20. This pulse compression process can be formulated in a more general way.

3.7.1 General Pulse Compression Scheme

The general scheme for pulse compression of optical pulses was independently proposed by Gires and Tournois in 1964 [38] and Giordmaine *et al.* in 1968 [39]. The input pulse is first spectrally broadened by a phase modulator. The phase over the generated spectrum is hopefully in a form that can be conveniently removed afterwards, i.e. all spectral components can be rephased to generate a short as possible pulse in the time domain. To compress femtosecond pulses an ultrafast phase modulator has to be used, that is the pulse has to modulate its phase itself by self-phase modulation. In 1969 Fisher *et al.* [40] proposed that picosecond pulses can be compressed to femtosecond duration using the large positive chirp produced around the peak of a short pulse by SPM in an optical Kerr liquid. In the same year Laubereau [41] used several cells containing CS_2 and a pair of diffraction gratings to compress, by approximately ten times, 20-ps pulses generated by a mode-locked Nd:glass laser.

As discussed in section 3.2, the optical Kerr effect in a medium gives rise to an intensity dependent change of the refractive index $\Delta n = n_{2,L} I(t)$, where $n_{2,L}$ is the nonlinear-index coefficient and $I(t)$ is the optical intensity. The self-induced intensity-dependent nonlinear phase shift experienced by an optical field during its propagation in a Kerr medium of length ℓ is given by $\Delta\phi(t) = -(\omega_0/c) n_2 I(t) \ell$ where ω_0 is the carrier frequency of the pulse. The induced frequency sweep over the pulse can be calculated from

Figure 3.13: Intensity profile, spectrum, instantaneous frequency, optimum quadratic compression and ideal compression for two cases: top row for a short fiber, i.e. high nonlinearity and low dispersion; bottom row optimum nonlinearity and dispersion.[42]

$\Delta\omega = d\Delta\phi/dt$, see Figure 3.13. Around the central part of the pulse, where most of the energy is concentrated, the phase is parabolic, leading to an approximately linear chirp in frequency. The region with linear chirp can be enlarged in the presence of positive dispersion in a Kerr medium of the same sign [42]. To compress the spectrally broadened and chirped pulse, a dispersive delay line can be used, characterized by a nearly linear group delay $T_g(\omega)$. Or if the chirp generated over the newly generated spectrum is nonlinear this chirp needs to be removed by a correspondingly nonlinear group delay $T_g(\omega)$. Figure 3.13 shows that in the case SPM and positive GDD a smoother spectrum with more linear chirp is created and therefore the final compressed pulse is of higher quality, i.e. a higher percentage of the total pulse energy is really concentrated in the short pulse and not in a large uncompressed pulse pedestal.

For a beam propagating in a homogenous medium,unfortunately the nonlinear refractive index does not only lead to a temporal phase modulation but also to a spatial phase modulation, which leads to self-focusing or defocusing and small-scale instabilities [43]. Therefore, a fundamental requirement

for pulse compression is that the Kerr effect is provided by a guiding nonlinear medium so that a spatially uniform spectral broadening is obtained. In 1974 Ippen *et al.* reported the first measurement of SPM in the absence of self-trapping and self-focusing by using a guiding multimode optical fiber filled with liquid CS_2 [44]. In 1978 Stolen and Lin reported measurements of SPM in single-mode silica core fibers [45]. The important advantage of the single-mode fiber is that the phase modulation can be imposed over the entire transverse profile of the beam, thus removing the problem of unmodulated light in the wings of the beam [44]. In 1981 Nakatsuka *et al.* [42] performed the first pulse compression experiment using fibers as a Kerr medium in the positive dispersion region.

3.7.2 Spectral Broadening with Guided Modes

The electric field of a guided mode can be written as [52]:

$$E(\mathbf{r},\omega) = A(z,\omega)F(x,y)\exp[i\beta(\omega)z] \tag{3.77}$$

where $A(z,\omega)$ is the mode-amplitude for a given frequency component, $F(x,y)$ is the mode-transverse field distribution and $\beta(\omega)$ is the mode-propagation constant. The propagation equation for the guided field splits into two equations for amplitude $A(z,\omega)$ and field pattern $F(x,y)$. In first order perturbation theory a perturbation $\Delta n = \bar{n}_2|E|^2$ of the refractive index, which is much smaller than the index step that defines the mode, does not change the modal distribution $F(x,y)$, while the mode propagation constant $\bar{\beta}(\omega)$ can be written as $\bar{\beta}(\omega) = \beta(\omega) + \Delta\beta$, where the perturbation $\Delta\beta$ is given by

$$\Delta\beta = \frac{(\omega_0/c)\int\int \Delta n|F(x,y)|^2 dxdy}{\int\int |F(x,y)|^2 dxdy}. \tag{3.78}$$

As shown by Eq.(3.78), the perturbation $\Delta\beta$, which includes the effect due to the fiber nonlinearity, is related to a spatial average on the fiber transverse section of the perturbation Δn. In this way, spatially uniform SPM is realized.

Using regular single mode fibers and prism-grating compressors, pulses as short as 6 fs at 620 nm were obtained in 1987 from 50-fs pulses generated by a colliding-pulse mode-locking dye laser [46] see Figure 3.14. More recently, 13-fs pulses from a cavity-dumped Ti:sapphire laser were compressed to 4.5

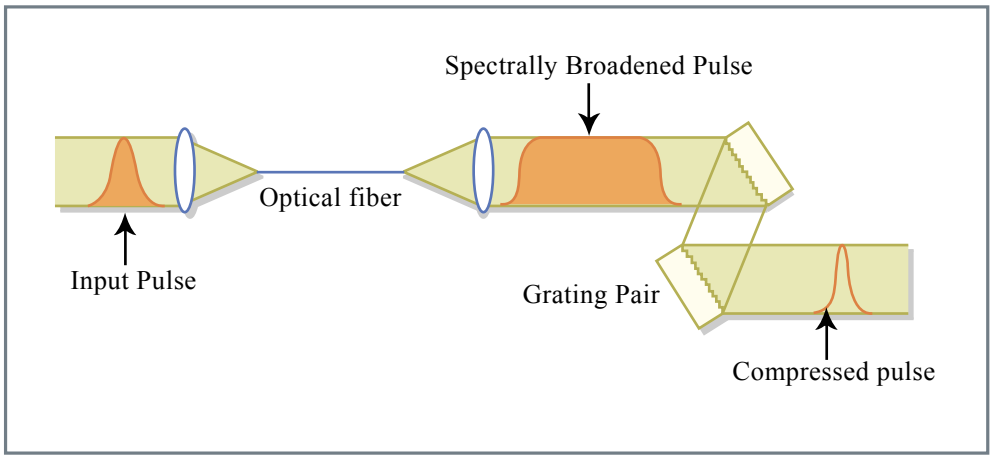

Figure 3.14: Fiber-grating pulse compressor to generate femtosecond pulses [53]

Figure by MIT OCW.

fs with the same technique using a compressor consisting of a quartz 45°-prism pair, broadband chirped mirrors and thin-film Gires-Tournois dielectric interferometers [47, 54]. The use of a single-mode optical fiber limits the pulse energy to a few nanojoule.

In 1996, using a phase modulator consisting of a hollow fiber (leaky waveguide) filled with noble gas, a powerful pulse compression technique has been introduced, which handles high-energy pulses [48]. The implementation of the hollow-fiber compression technique using 20-fs seed pulses from a Ti:sapphire system and chirped-mirrors that form a dispersive delay line has led to the generation of pulses with duration down to 4.5 fs [49] and energy up to 0.55 mJ [50]. This technique presents the advantages of a guiding element with a large-diameter mode and of a fast nonlinear medium with high damage threshold.

The possibility to take advantage of the ultrabroadband spectrum which can be generated by the phase modulation process, is strictly related to the development of dispersive delay lines capable of controlling the frequency-dependent group delay over such bandwidth.

3.7.3 Dispersion Compensation Techniques

The pulse frequency sweep (chirp) imposed by the phase modulation is approximately linear near the peak of the pulse, where most of the energy is concentrated. In the presence of dispersion in the phase modulator the chirp becomes linear over almost the whole pulse. Therefore, optimum temporal compression requires a group delay, $T_{g,comp}(\omega) = \partial\phi/\partial\omega$, characterized by a

nearly linear dependence on frequency in the dispersive delay line. Since in the case of SPM the nonlinear index n_2 is generally positive far from resonance, a negative group delay dispersion ($GDD = \partial T_g/\partial\omega$) is required in the compressor. In order to generate the shortest pulses, the pulse group delay after the phase modulator and the compressor must be nearly frequency independent. $T_g(\omega)$ can be expanded into a Taylor series around the central frequency ω_0:

$$T_g(\omega) = \phi'(\omega_0) + \phi''(\omega_0)\Delta\omega + \frac{1}{2}\phi'''(\omega_0)\Delta\omega^2 + \frac{1}{3!}\phi''''(\omega_0)\Delta\omega^3 + \cdots \quad (3.79)$$

where $\Delta\omega = \omega - \omega_0$, and $\phi''(\omega_0)$, $\phi'''(\omega_0)$, and $\phi''''(\omega_0)$ are the second-, the third-, and the fourth-order-dispersion terms, respectively. Critical values of these dispersion terms above which dispersion causes a significant change of the pulse are given by a simple scaling expression: $\phi^{(n)} = \tau_p^n$, where $\phi^{(n)}$ is the nth-order dispersion term and τ_p is the pulse duration. For example, a second order dispersion with $\phi'' = \tau_p^2$ results in a pulse broadening by more than a factor of two. Therefore dispersion-induced pulse broadening and distortion become increasingly important for decreasing pulse durations. Equation (3.79) shows that to compress a pulse to near the transform limit one should eliminate these high order dispersion terms. For instance, assuming a transform-limited input pulse to the phase modulator, the condition for third-order-dispersion-compensated compression is the following:

$$\phi''(\omega_0) = \phi''_{modulator} + \phi''_{compresssor} = 0 \quad (3.80)$$

$$\phi'''(\omega_0) = \phi'''_{modulator} + \phi'''_{compresssor} = 0 \quad (3.81)$$

Several compressor schemes have been developed so far that included such components as: diffraction gratings, Brewster-cut prism pairs, combination of gratings and prisms, thin prisms and chirped mirrors, and chirped mirrors only, etc. In the following we will briefly outline the main characteristics of these compressor schemes.

Grating and Prism Pairs

In 1968 Treacy demonstrated for the first time the use of a pair of diffraction gratings to achieve negative GDD [55]. In 1984 Fork et al. obtained negative GDD with pairs of Brewster-angled prisms [56]. Prism pairs have been widely used for dispersion control inside laser oscillators since they can be very low

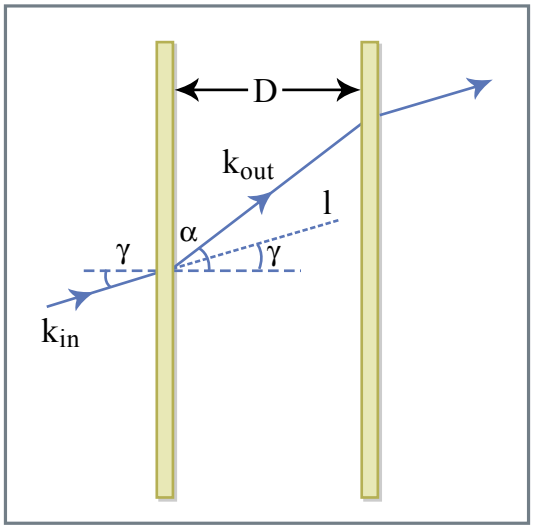

Figure 3.15: Optical path difference in a two-element dispersive delay line [107]

Figure by MIT OCW.

loss in contrast to grating pairs. In both optical systems the origin of the adjustable dispersion is the angular dispersion that arises from diffraction and refraction, respectively. The dispersion introduced by these systems can be easily calculated, by calculating the phase accumulated between the input and output reference planes [78]. To understand the main properties of these systems, we will refer to Fig. 3.15. The first element scatters the input beam with wave vector $\mathbf{k}_{in}$ and input path vector $\mathbf{l}$ into the direction $\mathbf{k}_{out}$. The beam passes between the first and the second element and is scattered back into its original direction. The phase difference by the scattered beam and the reference beam without the grating is: $\phi(\omega) = \mathbf{k}_{out}(\omega) \cdot \mathbf{l}$. Considering free-space propagation between the two elements, we have $|\mathbf{k}_{out}| = \omega/c$, and the accumulated phase can be written as

$$\phi(\omega) = \frac{\omega}{c}|\mathbf{l}|\cos[\gamma - \alpha(\omega)] = \frac{\omega}{c}\frac{D}{\cos(\gamma)}\cos[\gamma - \alpha(\omega)] \tag{3.82}$$

where: γ is the angle between the incident wave vector and the normal to the first element; α is the angle of the outgoing wave vector, which is a function of frequency; D is the spacing between the scattering elements along a direction parallel to their normal. In the case of a grating pair the frequency dependence of the diffraction angle α is governed by the grating

law, that in the case of first-order diffraction is given by:

$$\frac{2\pi c}{\omega} = d[\sin\alpha(\omega) - \sin\gamma] \tag{3.83}$$

where d is the groove spacing of the grating. Using Eq.(3.82) and Eq.(3.83), it is possible to obtain analytic expressions for the GDD and the higher-order dispersion terms (for single pass):

$$\phi''(\omega) = -\frac{4\pi^2 cD}{\omega^3 d^2 \cos^3\alpha(\omega)} \tag{3.84}$$

$$\phi'''(\omega) = \frac{12\pi^2 cD}{\omega^4 d^2 \cos^3\alpha(\omega)}\left(1 + \frac{2\pi c \sin\alpha(\omega)}{\omega d \cos^2\alpha(\omega)}\right) \tag{3.85}$$

It is evident from Eq.(3.84) that grating pairs give negative dispersion. D is the distance between the gratings. A disadvantage of the grating pair is the diffraction loss. For a double-pass configuration the loss is typically 75%. Also the bandwidth for efficient diffraction is limited.

In the case of a Brewster-angled prism pair Eq.(3.82) reduces to the following expression (for single pass) [56]:

$$\phi(\omega) = \frac{\omega}{c}\ell_p \cos\beta(\omega) \tag{3.86}$$

where ℓ_p is the distance between prism apices and $\beta(\omega)$ is the angle between the refracted ray at frequency ω and the line joining the two apices. The second and third order dispersion can be expressed in terms of the optical path $P(\lambda) = \ell_p \cos\beta(\lambda)$:

$$\phi''(\omega) = \frac{\lambda^3}{2\pi c^2}\frac{d^2P}{d\lambda^2} \tag{3.87}$$

$$\phi'''(\omega) = -\frac{\lambda^4}{4\pi^2 c^3}\left(3\frac{d^2P}{d\lambda^2} + \lambda\frac{d^3P}{d\lambda^3}\right) \tag{3.88}$$

with the following derivatives of the optical path with respect to wavelength evaluated at Brewster's angle:

$$\frac{d^2P}{d\lambda^2} = 2[n'' + (2n - n^{-3})(n')^2]\ell_p \sin\beta - 4(n')^2\ell_p\cos\beta \tag{3.89}$$

$$\frac{d^3P}{d\lambda^3} = [6(n')^3(n^{-6} + n^{-4} - 2n^{-2} + 4n^2) + 12n'n''(2n - n^{-3}) \tag{3.90}$$

$$+2n''']\ell_p \sin\beta + 12[(n^{-3} - 2n)(n')^3 - n'n'']\ell_p\cos\beta \tag{3.91}$$

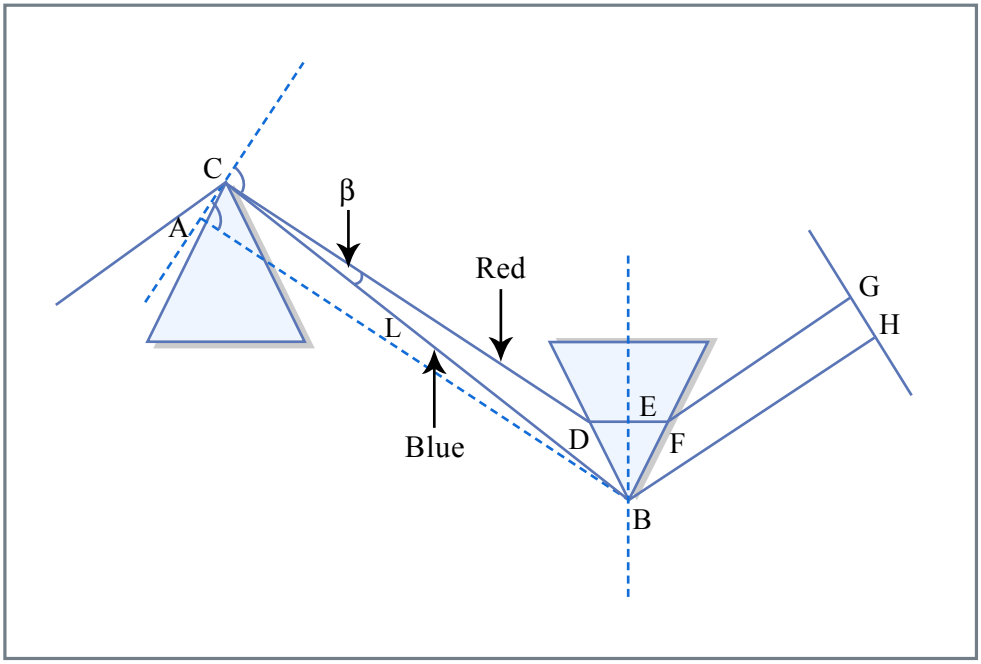

Figure 3.16: Prism pair for dispersion compensation. The blue wavelengths have less material in the light path then the red wavelengths. Therefore, blue wavelengths are less delayed than red wavelength

Figure by MIT OCW.

where n is the refractive index of the prism material; n', n'' and n''' are respectively, the first-, second- and third-order derivatives of n, with respect to wavelength. The prism-compressor has the advantage of reduced losses. Using only fused silica prisms for dispersion compensation, sub-10-fs light pulses have been generated directly from an oscillator in 1994 [79]. In 1996, pulses with tens of microjoules energy, spectrally broadened in a gas-filled hollow fiber were compressed down to 10 fs using a prism compressor [48]. Both in the case of grating and prism pairs, negative GDD is associated with a significant amount of higher-order dispersion, which cannot be lowered or adjusted independently of the desired GDD, thus limiting the bandwidth over which correct dispersion control can be obtained. This drawback has been only partially overcome by combining prism and grating pairs with third-order dispersion of opposite sign. In this way pulses as short as 6 fs have been generated in 1987 [46], and less than 5 fs in 1997 [47], by external compression. This combination cannot be used for few-optical-cycle pulse generation either in laser oscillators, due to the high diffraction losses of the gratings, or in external compressors at high power level, due to the onset of

unwanted nonlinearities in the prisms.

3.7.4 Dispersion Compensating Mirrors

Chirped mirrors are used for the compression of high energy pulses, because they provide high dispersion with little material in the beam path, thus avoiding nonlinear effects in the compressor.

Grating and prism compressors suffer from higher order dispersion. In 1993 Robert Szipoecs and Ferenc Krausz [80] came up with a new idea, so called chirped mirrors. Laser mirrors are dielectric mirrors composed of alternating high and low index quarter wavelenth thick layers resulting in strong Bragg-reflection. In chirped mirrors the Bragg wavelength is chirped so that different wavelength penetrate different depth into the mirror upon reflection giving rise to a wavelength dependent group delay. It turns out that the generation of few-cycle pulses via external compression [95] as well as direct generation from Kerr lens mode-locked lasers [58] relies heavily on the existence of chirped mirrors [57, 83, 59] for dispersion compensation. There are two reasons to employ chirped mirrors . First the high-reflectivity bandwidth, Δf, of a standard dielectric Bragg-mirror is determined by the Fresnel reflectivity r_B of the high, n_H, and low, n_L, index materials used for the dielectric mirror

$$r_B = \frac{\Delta f}{f_c} = \frac{n_H - n_L}{n_H + n_L} \tag{3.92}$$

where f_c is again the center frequency of the mirror. Metal mirrors are in general too lossy, especially when used as intracavity laser mirrors. For material systems typically used for broadband optical coatings such as Silicon Dioxide and Titanium Dioxide with $n_{SiO_2} = 1.48$ and $n_{TiO_2} = 2.4$, (these indexes might vary depending on the deposition technique used), a fractional bandwidth $\Delta f/f_c = 0.23$ can be covered. This fractional bandwidth is only about a third of an octave spanning mirror $\Delta f/f_c = 2/3$. Furthermore, the variation in group delay of a Bragg-mirror impacts already pulses that fill half the spectral range $\Delta f = 0.23 f_c$. A way out of this dilemma was found by introducing chirped mirrors [57], the equivalent of chirped fiber Bragg gratings, which at that time were already well developed components in fiber optics [60]. When the Bragg wavelength of the mirror stack is varied slowly enough and no limitation on the number of layer pairs exists, an arbitrary high reflectivity range of the mirror can be engineered. The second reason for using chirped mirrors is based on their dispersive properties due to the

wavelength dependent penetration depth of the light reflected from different positions inside the chirped multilayer structure. Mirrors are filters, and in the design of any filter, the control of group delay and group delay dispersion is difficult. This problem is further increased when the design has to operate over wavelength ranges up to an octave or more.

The matching problem Several designs for ultra broadband dispersion compensating mirrors have been developed over the last years. For dispersion compensating mirrors which do not extend the high reflectivity range far beyond what a Bragg-mirror employing the same materials can already achieve, a multi-cavity filter design can be used to approximate the desired phase and amplitude properties [61, 62]. For dispersion compensating mirrors covering a high reflectivity range of up to $\Delta f/f_c = 0.4$ the concept of double-chirped mirrors (DCMs) has been developed [83][81]. It is based on the following observations. A simple chirped mirror provides high-reflectivity over an arbitrary wavelength range and, within certain limits, a custom designable average group delay via its wavelength dependent penetration depth [73] (see Figure 3.17 (a) and (b)). However, the group delay as a function of frequency shows periodic variations due to the impedance mismatch between the ambient medium and the mirror stack, as well as within the stack (see Figure 3.17 b and Figure 3.18). A structure that mitigates these mismatches and gives better control of the group delay dispersion (GDD) is the double-chirped mirror (DCM) (Figure 3.17 c), in a way similar to that of an apodized fiber Bragg grating [64].

Figure 3.18 shows the reflectivity and group delay of several Bragg and chirped mirrors composed of 25 index steps, with $n_H = 2.5$ and $n_L = 1.5$, similar to the refractive indices of TiO_2 and SiO_2, which result in a Fresnel reflectivity of $r_B = 0.25$. The Bragg-mirror can be decomposed in symmetric index steps [83]. The Bragg wavenumber is defined as $k_B = \pi/(n_L d_L + n_H d_H)$, where d_L and d_H are the thicknesses of the low and high index layer, respectively. The Bragg wavenumber describes the center wavenumber of a Bragg mirror composed of equal index steps. In the first case, (Figure 3.18, dash-dotted line) only the Bragg wave number is linearly chirped from $6.8\mu m^{-1} < k_B < 11\mu m^{-1}$ over the first 20 index steps and held constant over the last 5 index steps. The reflectivity of the structure is computed assuming the structure imbedded in the low index medium. The large oscillations in the group delay are caused by the different impedances of the chirped

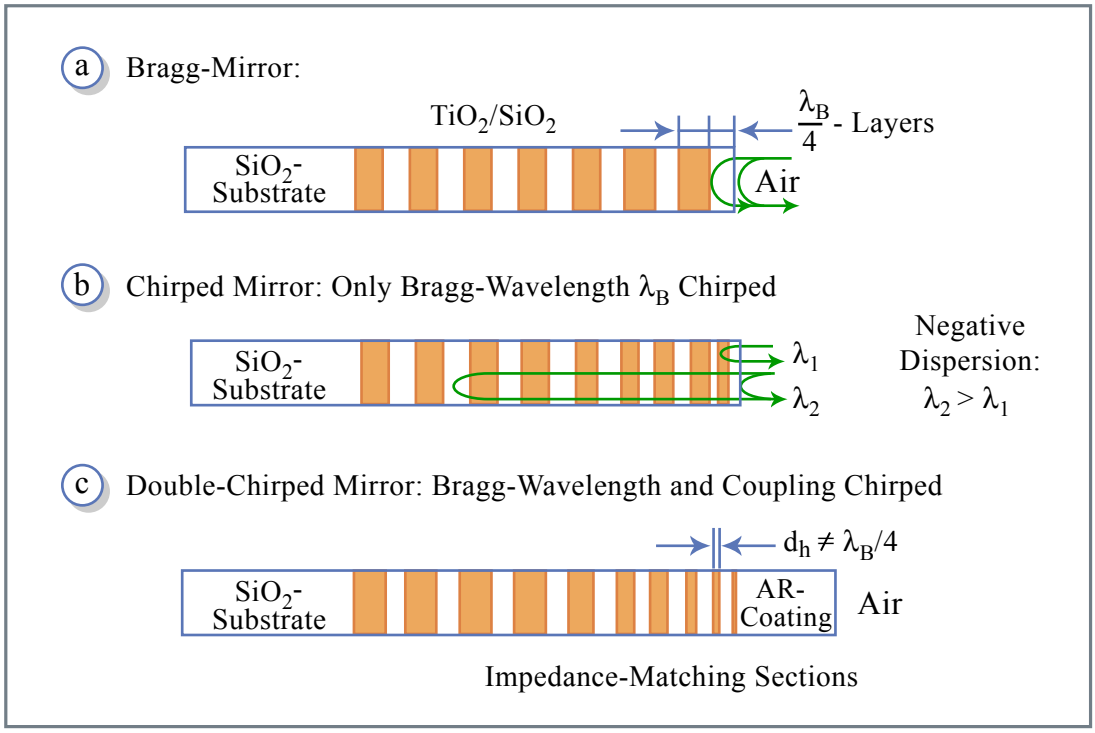

Figure 3.17: a) Standard Bragg mirror; (b) Simple chirped mirror, (c) Double-chirped mirror with matching sections to avoid residual reflections causing undesired oscillations in the GD and GDD of the mirror.

Figure by MIT OCW.

grating and the surrounding low index material causing a strong reflection at the interface of the low index material and the grating stack. By adiabatic matching of the grating impedance to the low index material this reflection can be avoided. This is demonstrated in Fig. 3.18 by the dashed and solid curves, corresponding to an additional chirping of the high index layer over the first 12 steps according to the law $d_H = (m/12)^\alpha \lambda_{B,12}/(4n_H)$ with $\alpha = 1$, and 2, for linear and quadratic adiabatic matching. The argument m denotes the m-th index step and $\lambda_{B,12} = 0.740\mu m$. The strong reduction of the oscillations in the group delay by the double-chirp technique is clearly visible. Quadratic tapering of the high index layer, and therefore, of the grating already eliminates the oscillations in the group delay completely, which can also be shown analytically by coupled mode analysis [81]. Because of the double chirp a high transmission window at the short wavelength end of the mirror opens up which is ideally suited for the pumping of Ti:sapphire lasers. So far, the double-chirped mirror is only matched to the low index material of the mirror. Ideally, the matching can be extended to any other ambient medium by a properly designed AR-coating. However, this AR-coating has to be of very high quality, i.e. very low residual reflectivity ideally a power

Figure 3.18: Comparison of the reflectivity and group delay of chirped mirrors with 25 layer pairs and refractive indices $n_H = 2.5$, and $n_L = 1.5$.The upper portion shows the enlarged top one percent of the reflectivity. The dotted curves show the result for a simple chirped mirror. The dashed and solid curves show the result for double-chirped mirrors where in addition to the chirp in the Bragg wave number k_B the thickness of the high-index layers is also chirped over the first 12 layer pairs from zero to its maximum value for a linear chirp, i.e. $\alpha = 1$, (dashed curves) and for a quadratic chirp, i.e. $\alpha = 2$ (solid curves). [83].

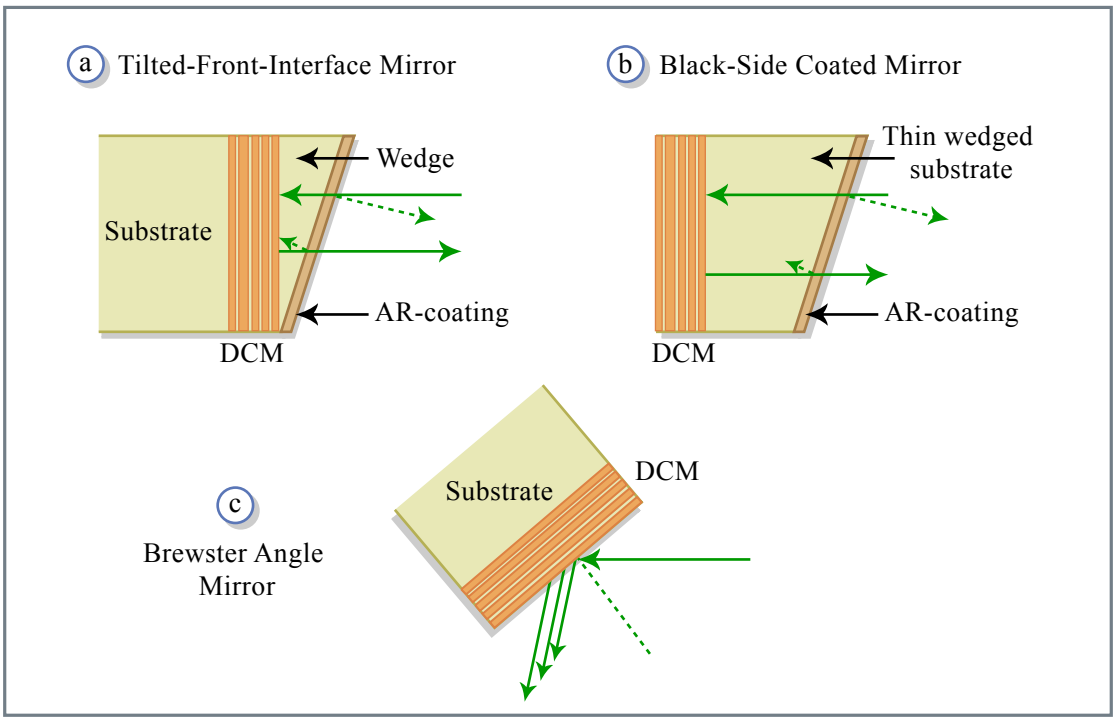

Figure 3.19: Schematic structure of proposed broadband dispersion compensating mirror system avoiding the matching to air: (a) tilted-front-interface mirror; (b) back-side coated mirror and (c) Brewster-angle mirror.

Figure by MIT OCW.

reflectivity of 10^{-4}, i.e. an amplitude reflectivity of $r = 10^{-2}$ is required. The quality of the AR-coating can be relaxed, if the residual reflection is directed out of the beam path. This is achieved in so called tilted front-side or back-side coated mirrors [65], [66], (Fig. 3.19 (a) and (b)). In the back-side coated mirror the ideal DCM structure, which is matched to the low index material of the mirror is deposited on the back of a substrate made of the same or at least very similar low index material. The AR-coating is deposited on the front of the slightly wedged substrate, so that the residual reflection is directed out of the beam and does not affect the dispersion properties. Thus the task of the AR-coating is only to reduce the Fresnel losses of the mirror at the air-substrate interface, and therefore, it is good enough for some applications, if the residual reflection at this interface is of the order of 0.5%. However, the substrate has to be very thin in order to keep the overall mirror dispersion negative, typically on the order of 200-500 μm. Laser grade quality optics are hard to make on such thin substrates and the stress induced by the coating leads to undesired deformation of the substrates. The front-side coated mirror overcomes this shortcoming

by depositing the ideal DCM-structure matched to the index of the wedge material on a regular laser grade substrate. A 100-200 μm thin wedge is bonded on top of the mirror and the AR-coating is then deposited on this wedge. This results in stable and octave spanning mirrors, which have been successfully used in external compression experiments [69]. Both structures come with limitations. First, they introduce a wedge into the beam, which leads to an undesired angular dispersion of the beam. This can partially be compensated by using these mirrors in pairs with oppositely oriented wedges. The second drawback is that it seems to be impossible to make high quality AR-coatings over one or more than one octave of bandwidth, which have less than 0.5% residual reflectivity [68], i.e. on one reflection such a mirror has at least 1% of loss, and, therefore, such mirrors cause high losses inside a laser. For external compression these losses are acceptable. A third possibility for overcoming the AR-coating problem is given by using the ideal DCM under Brewster-angle incidence, (Figure 3.19) [67]. In that case, the low index layer is automatically matched to the ambient air. However, under p-polarized incidence the index contrast or Fresnel reflectivity of a layer pair is reduced and more layer pairs are necessary to achieve high reflectivity. Also the penetration depth into the mirror increased, so that scattering and other losses in the layers become more pronounced. On the other hand, such a mirror can generate more dispersion per bounce due to the higher penetration depth. For external compression such mirrors might have advantages because they can cover bandwidths much wider than one octave. This concept is difficult to apply to the fabrication of curved mirrors. There is also a spatial chirp of the reflected beam, which may become sizeable for large penetration depth and has to be removed by back reflection or an additional bounce on another Brewster-angle mirror, that recombines the beam. For intracavity mirrors a way out of this dilemma is found by mirror pairs, which cancel the spurious reflections due to an imperfect AR-coating and matching structure in the chirped mirror [76]. Also this design has its drawbacks and limitations. It requires a high precision in fabrication and depending on the bandwidth of the mirrors it may be only possible to use them for a restricted range of angles of incidence.

Double-chirped mirror pairs

There have been several proposals to increase the bandwidth of laser mirrors by mutual compensation of GDD oscillations [70, 71, 72] using computer

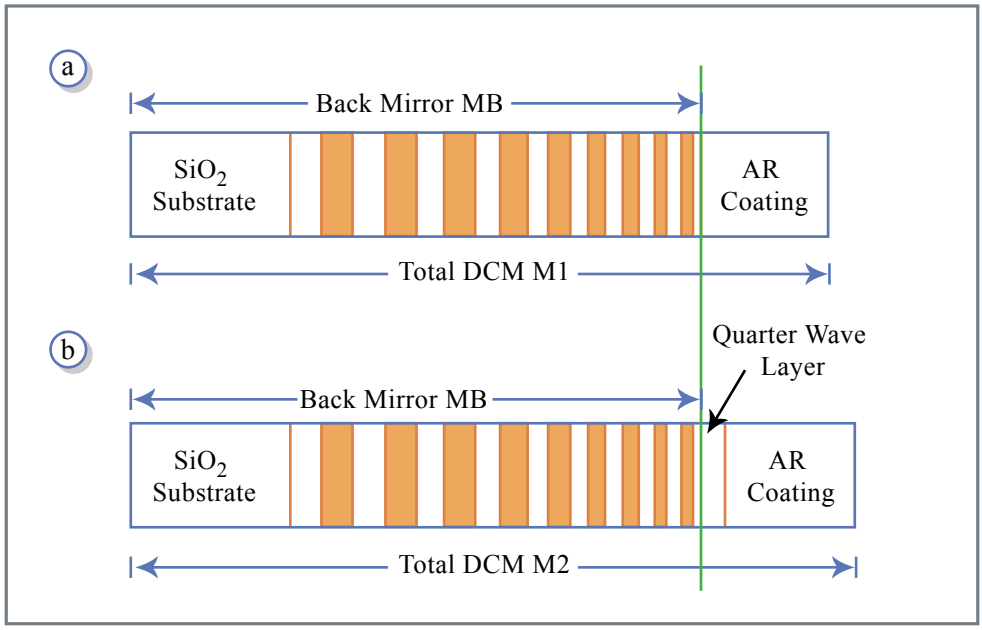

Figure 3.20: DCM-Pair M1 (a) and M2 (b). The DCM M1 can be decomposed in a double-chirped back-mirror MB matched to a medium with the index of the top most layer. In M2 a layer with a quarter wave thickness at the center frequency of the mirror and an index equivalent to the top most layer of the back-mirror MB is inserted between the back-mirror and the AR-coating. The new back-mirror comprising the quarter wave layer can be reoptimized to achieve the same phase as MB with an additional π-phase shift over the whole octave of bandwidth.

Figure by MIT OCW.

optimization. These early investigations resulted in a rather low reflectivity of less than 95% over almost half of the bandwidth considered. The ideas leading to the DCMs help us to show analytically that a design of DCM-pairs covering one octave of bandwidth, i.e. 600 nm to 1200 nm, with high reflectivity and improved dispersion characteristics is indeed possible [76]. Use of these mirror pairs in a Ti:sapphire laser system resulted in 5 fs pulses with octave spanning spectra directly from the laser [58]. Yet, the potential of these pairs is by no means fully exploited.

A DCM-Pair, see Fig. 3.20, consists of a mirror M1 and M2. Each is composed of an AR-coating and a low-index matched double-chirped back-mirror MB with given wavelength dependent penetration depth. The high reflectivity range of the back-mirror can be easily extended to one octave by simply chirping slowly enough and using a sufficient number of layer pairs.

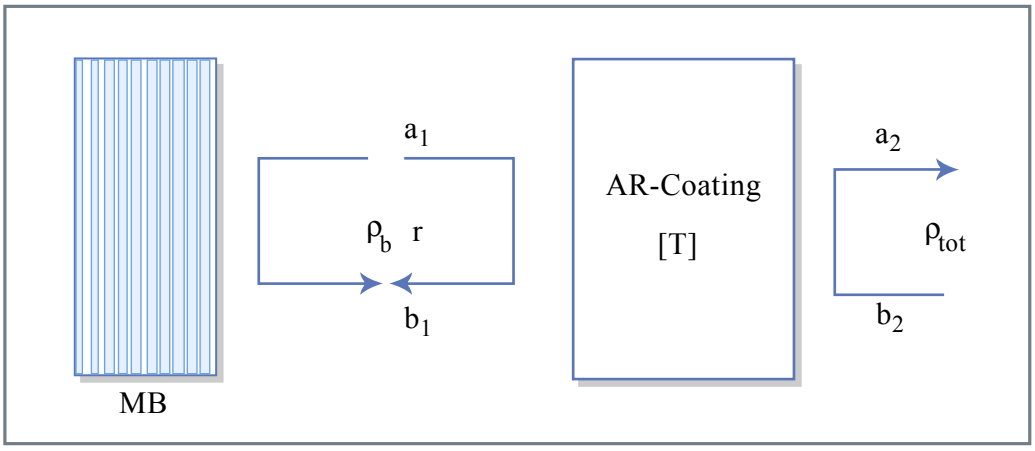

Figure 3.21: Decomposition of a DCM into a double-chirped backmirror MB and an AR-coating.

Figure by MIT OCW.

However, the smoothness of the resulting GDD strongly depends on the quality of matching provided by the AR-coating and the double-chirped section. Fig. 3.21 indicates the influence of the AR-coating on the GDD of the total DCM-structure. The AR-coating is represented as a two - port with two incoming waves a_1, b_2 and two outgoing waves a_2, b_1. The connection between the waves at the left port and the right port is described by the transfer matrix

$$\begin{pmatrix} a_1 \\ b_1 \end{pmatrix} = T_{ar} \begin{pmatrix} a_2 \\ b_2 \end{pmatrix} \quad \text{with} \quad T_{ar} = \begin{pmatrix} \frac{1}{t} & \frac{r^*}{t^*} \\ \frac{r}{t} & \frac{1}{t^*} \end{pmatrix} \tag{3.93}$$

where we assumed that the multilayer AR-coating is lossless. Here, r and t are the complex coefficients for reflection and transmission at port 1 assuming reflection free termination of port 2. The back-mirror MB, is assumed to be perfectly matched to the first layer in the AR-coating, has full reflection over the total bandwidth under consideration. Thus its complex reflectivity in the range of interest is given by

$$\rho_b = e^{j\phi_b(\omega)} \tag{3.94}$$

The phase $\phi_b(\omega)$ is determined by the desired group delay dispersion

$$GDD_b = -d^2\phi_b(\omega)/d\omega^2 \tag{3.95}$$

up to an undetermined constant phase and group delay at the center frequency of the mirror, ω_c. All higher order derivatives of the phase are determined by the desired dispersion of the mirror. Analytic formulas for the design of DCMs, showing custom designed dispersion properties without considering the matching problem to the ambient air, can be found in [73].

The resulting total mirror reflectivity including the AR-coating follows from (3.93)

$$\rho_{tot} = \frac{t}{t^*}\rho_b \frac{1 - r^*/\rho_b}{1 - r\rho_b} \tag{3.96}$$

For the special case of a perfectly reflecting back-mirror according to Eq. (3.94) we obtain

$$\rho_{tot} = \frac{t}{t^*} e^{j\phi_b(\omega)} \frac{1 - z^*}{1 - z}, \quad \text{with} \quad z = re^{j\phi_b(\omega)} \tag{3.97}$$

The new reflectivity is again unity but new contributions in the phase of the resulting reflectivity appear due to the imperfect transmission properties of the AR-coating. With the transmission coefficient of the AR-coating

$$t = |t|e^{j\phi_t}, \tag{3.98}$$

The total phase of the reflection coefficient becomes

$$\phi_{tot} = 2\phi_t + \phi_b(\omega) + \phi_{GTI} \tag{3.99}$$

with

$$\phi_{GTI} = 2\arctan\left[\frac{Im\{z\}}{1 + Re\{z\}}\right] \tag{3.100}$$

Here, ϕ_t is the phase of the transmission coefficient and ϕ_{GTI} is the phase due to the Gire-Tournois interferometer created by the non-perfect AR-coating, i.e. $r \neq 0$, and the back-mirror MB, (Figure 3.21). The phase ϕ_t of a good AR-coating, i.e. $|r| < 0.1$, is linear and, therefore, does not introduce undesired oscillations into the GD and GDD. However, the phase ϕ_{GTI} is rapidly varying since $\phi_b(\omega)$ varies over several 2π over the frequency range of interest due to the monotonic group delay of the back-mirror. The size of these oscillations scale with the quality of the AR-coating, i.e. with $|r|$. Thus, the GDD oscillations are reduced with smaller residual reflectivity of the AR-coating. Assuming, that the reflectivity r is real and smaller or equal to 0.1, the oscillations in the group delay and group delay dispersion are easily estimated by

$$T_{g,GTI} = \frac{d\phi_{GTI}}{d\omega} \approx -rT_{gb}(\omega)\cos[\phi_b(\omega)] \tag{3.101}$$

with

$$\begin{aligned} T_{gb}(\omega) &= -d\phi_b(\omega)/d\omega, \\ GDD_{GTI} &= \tfrac{d^2\phi_{GTI}}{d\omega^2} \\ &\approx r\left(T_{gb}^2(\omega)\sin[\phi_b(\omega)] - GDD_b\cos[\phi_b(\omega)]\right) \end{aligned} \tag{3.102}$$

The GTI-reflections add up coherently when multiple reflections on chirped mirrors occur inside the laser over one round-trip, leading to pre- and post pulses if the mode-locking mechanism is not strong enough to suppress them sufficiently. Experimental results indicate that a residual reflection in the AR-coating of $r < 0.01$ and smaller, depending on the number of reflections per round-trip, is required so that the pre- and post pulses are sufficiently suppressed. This corresponds to an AR-coating with less than 10^{-4} residual power reflectivity, which can only be achieved over a very limited range, as discussed above.

Over a limited wavelength range of 350 nm centered around 800 nm low residual power reflectivities as small as 10^{-4} have been achieved effectively after reoptimization of the AR-coating section and the double-chirped section to form a combined matching section of higher matching quality. For even larger bandwidth, approaching an octave, a residual power reflectivity of 10^{-4} is no longer possible [68]. A way out of this limitation is offered by the observation, that a coherent subtraction of the pre- and post-pulses to first order in r is possible by reflections on a mirror pair M1 and M2, see Figure 3.20 (a) and (b). A series of two reflections on a mirror with reflectivity (3.97) and on a similar mirror with an additional phase shift of π between the AR-coating and the back-mirror, having a reflectivity (3.97) where z is replaced by $-z$, leads to a coherent subtraction of the first order GTI-effects. The resulting total reflectivity of the two reflections is given by the product of the individual complex reflectivities assuming the same AR-coating

$$\rho_{tot,2} = -\left(\frac{t}{t^*}\right)^2 e^{i2\phi_b(\omega)} \frac{1-z^{*2}}{1-z^2} \tag{3.103}$$

Now, the GTI-effects scale like the power reflectivity of the AR-coating r^2 instead of the amplitude reflectivity r, which constitutes a tremendous improvement, since it is possible to design AR-coatings to the low index material $Si0_2$ of the mirror with a residual power reflectivity between 0.001 and 0.01 while covering one octave of bandwidth [68]. However, there does not exist a single physical layer which generates a phase shift of $\pi/2$ during one passage for all frequency components contained in an octave. Still, a layer with a quarter wave thickness at the center frequency is a good starting design. Then the back-mirror MB in the Mirror M2 can be reoptimized to take care of the deviation from a quarter wave thickness further away from the center frequency, because the back-mirror acts as a highly dispersive medium where the phase or group delay can be designed at will.

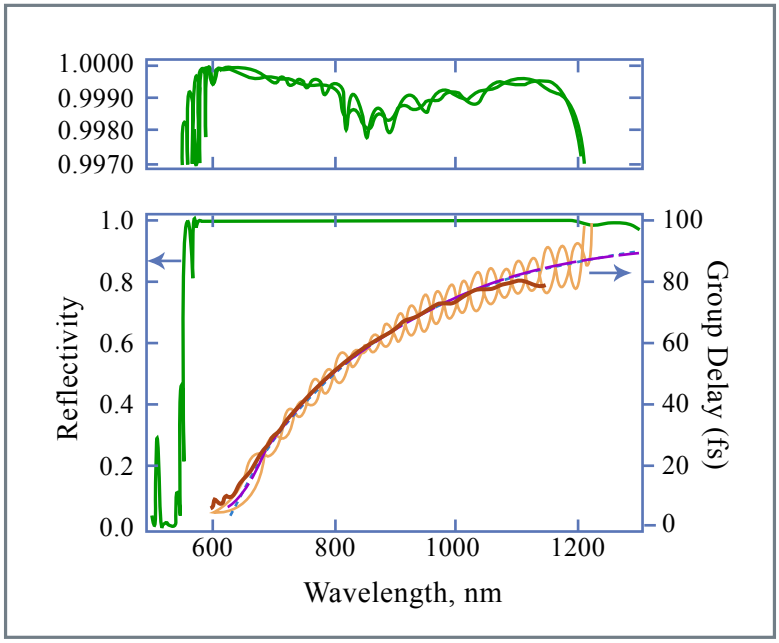

Figure 3.22: Reflectivity of the mirror with pump window shown as thick solid line with scale to the left. The group delay design goal for perfect dispersion compensation of a prismless Ti:sapphire laser is shown as thick dash-dotted line with scale to the right. The individual group delay of the designed mirrors is shown as thin line and its average as a dashed line, which is almost identical with the design goal over the wavelength range form 650-1200 nm. The measured group delay, using white light interferometry, is shown as the thick solid line from 600-1100 nm. Beyond 1100nm the sensitivity of Si-detector used prevented further measurements.

Figure 3.23 shows in the top graph the designed reflectivity of both mirrors of the pair in high resolution taking into account the absorption in the layers. The graph below shows the reflectivity of the mirror, which has in addition high transmission between 510-550 nm for pumping of the Ti:sapphire crystal. Each mirror consists of 40 layer pairs of SiO_2 and TiO_2 fabricated using ion-beam sputtering [74, 75]. Both mirror reflectivities cover more than one octave of bandwidth from 580 nm to 1200 nm or 250 to 517 THz, with an average reflectivity of about 99.9% including the absorption in the layers. In addition, the mirror dispersion corrects for the second and higher order dispersion of all intracavity elements such as the Ti:sapphire crystal and the thin, small angle, BaF_2 wedges, for fine adjustment of the dispersion from 650 nm to 1200 nm within the 12 bounces occurring in one roundtrip. The choice for the lower wavelength boundary in dispersion compensation is determined and limited by the pump window of Ti:sapphire. The dispersion measurement was performed using white light interferometry [77], up to about 1100 nm because of the silicon detector roll-off. The oscillations in the group delay of each mirror are about 10 times larger than those of high quality DCMs covering 350 nm of bandwidth [**?**]. However, in the average group delay of both mirrors the oscillations are ideally suppressed due to cancellation by more than a factor of ten. Therefore, the effective residual reflectivity of the mirror pair covering one octave, r^2, is even smaller than that of conventional DCMs.

Methods for active dispersion compensation

Various schemes for active pulse compression have been developed based on the use of liquid-crystal modulators (LCM), acousto-optic modulators (AOM), and mechanically deformable mirrors.

Dispersion compensation using liquid crystal modulators A pulse shaping technique [84] based on the use of a LCM for pulse compression offers the advantage of a large bandwidth (300-1500 nm) and *in situ* adaptive phase control, see Figure3.23. In 1997 Yelin *et al.* [85] demonstrated an adaptive method for femtosecond pulse compression based on LCM. Strongly chirped 80-fs pulses generated by an oscillator were sent in a 4-f pulse shaper composed of a pair of thin holographic transmission gratings. A programmable one-dimensional LCM, placed in the Fourier plane of the shaper, was used as an updatable filter for pulse spectral manipulation. Pulses as short as

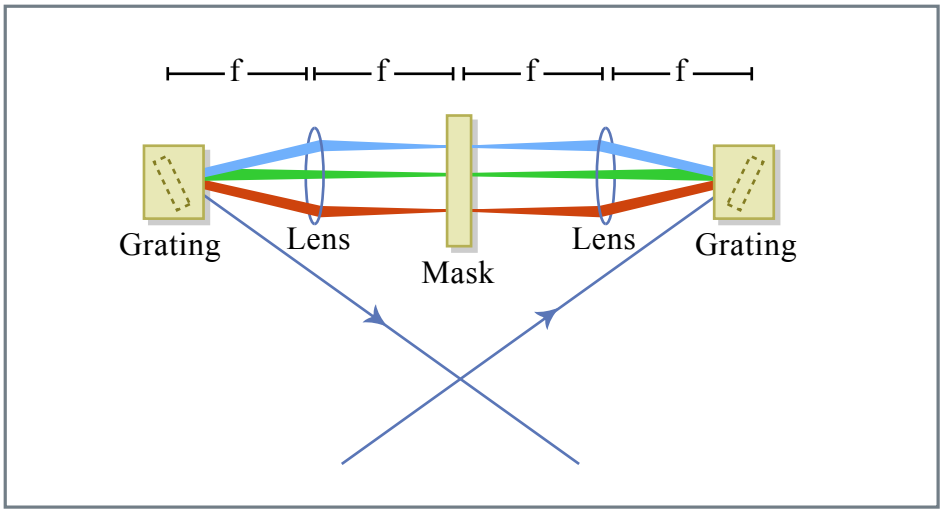

Figure 3.23: Grating Pair and LCM pulse shaper according to Weiner and Heritage [88]. To shape amplitude and phase two pulse shapers with an amplitude and phase mask each are necessary.

Figure by MIT OCW.

11 fs (transform-limited duration: 9 fs) have been obtained, employing an optimization algorithm for adaptive compression based on a search in the two-dimensional space of second- and third-order dispersion coefficients. In 2001, Karasawa *et al.* [86] demonstrated pulse compression, down to 5 fs, of broadband pulses from an argon-filled hollow fiber, using only a LCM for phase compensation. More recently [51], pulses as short as 3.8 fs have been achieved through a closed-loop combination of a liquid-crystal spatial light modulator for adaptive pulse compression and spectral-phase interferometry for direct electric-field reconstruction (SPIDER) [87] measurements as feedback signal.

One problem of the method is pixelization in the Fourier plane owing to the technology of the liquid-crystal active matrix. Diffraction on pixel edges and absorption by the black matrix introduce parasitic effects. The requirement that the actual spectral modulation should approximate a smooth function despite the fixed, finite size of the individual modulator elements, limits the temporal range over which pulse compression can be achieved [88]. Other problems are related to the optical damage of the LCM, which limits the maximum pulse energy, and to the high losses introduced by the device.

Various nonpixelated devices have been proposed: Dorrer *et al.* have reported on an optically addressed LCM (liquid crystal light valve) [89]. The light valve consists of two continuous transparent electrodes and continuous

layers of a nematic twisted liquid crystal and of photoconductive $Bi_{12}SiO_{20}$ (BSO). A local variation of illumination of the BSO layer (in the blue green spectral region) induces a change in conductivity. When a voltage is applied between the two electrodes, the variation of the BSO conductivity results in a change in the voltage drop across the liquid crystal layer. As the birefringence of the liquid crystal is voltage dependent, a local variation of the refractive index is created, which translates into a variation of the optical phase of the local spectral component. The light valve is addressed by using a display device. Pixelation effects are avoided because the light valve itself is a continuous device. The control of the light valve is more complicated than for the electrically addressed LCM. Moreover, due to its limited spatial frequency response, the spectral resolution is limited.

Dispersion compensation using acousto-optic modulators

In 1997 Tournois proposed an acousto-optic programmable dispersive filter (AOPDF), to provide large dispersion-compensation ranges[91]. The device is based on a collinear acousto-optic interaction in a birefringent uniaxial crystal, see Figure 3.24. The acoustic frequency is a variable function of time and provides control over the group delay of the diffracted optical pulse. At the same time, the spectral amplitude of the diffracted pulse is driven by the intensity of the acoustic signal. As demonstrated in Ref. [91], the optical output $E_{out}(t)$ of the AOPDF is proportional to the convolution of the optical input, $E_{in}(t)$, and the scaled acoustic signal:

$$E_{out}(t) \propto E_{in}(t) \otimes S(t/\alpha) \tag{3.104}$$

where the scaling factor $\alpha = \Delta n(V/c)$ is the ratio of the speed of sound to the speed of light times the index difference between the ordinary and the extraordinary waves. Therefore, by generating the proper function $S(t)$, it is possible to generate any arbitrary convolution with a temporal resolution given by the inverse of the filter bandwidth. Such device have been used in kilohertz chirped-pulse amplification laser chains compensating for gain narrowing and residual phase errors with the AOPDF, resulting in the generation of 17-fs transform-limited pulses [92]. The total throughput is 10-50%, depending on the bandwidth of the device. Devices approaching one octave in bandwidth are possible.

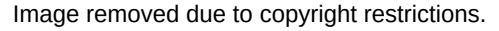

Figure 3.24: Acousto-optic programable pulse shaper. One element can shape amplitude and phase of the pulse.

Dispersion compensation using deformable mirrors

Mechanically deformable mirrors can be used for active dispersion control, as proposed by Heritage *et al.* [93]. More recently, pulse compression has been achieved using an electrostatically deformable, gold-coated, silicon nitride membrane mirror, placed in the Fourier plane of a $4f$ zero-dispersion stretcher [94]. The membrane was suspended over an array of 39 actuator electrodes. The potential applied to each actuator generates an electrostatic attraction between the membrane and the electrode, thus inducing a deformation of the mirror surface, which translates into a modulation of the phase of the spectral components of the input pulse. The total phase difference is $\phi = 2(2\pi)\Delta z/\lambda$, where Δz is the deflection of the mirror. The minimum radius of curvature of the mirror membrane is given by $R = T/P$, where T is the membrane tension and P is the maximum electrostatic pressure. This limitation of the membrane curvature restricts the possibility of the mirror correction of higher-order phases. The main advantages of this method are the following: the phase modulation is smoothly varying; reduced losses due to the high reflectivity (97%) of the mirror; relatively high actuator density. Experiments have been performed with a mode-locked Ti:sapphire laser, where the deformable mirror recompressed a 15 fs pulse, previously stretched to 90 fs by dispersion in glass, back to approximately the bandwidth limit [94].

Recently, dispersion control over a bandwidth of $\sim$ 220 THz has been demonstrated by A. Baltuška et al. [95] using a compressor consisting of a pair of chirped mirrors and a grating dispersion line with a computer-controlled flexible mirror positioned in the focal plane. The total throughput of the pulse shaper was less than 12% because of the low diffraction efficiency of the grating. Using this compressor, the visible-near-IR pulses, generated by optical parametric amplification, were compressed to a 4-fs duration.

3.7.5 Hollow Fiber Compression Technique

Single mode fiber only allows compression of low energy pulses. In 1996 the group of DeSilvestri in Milan [48] developed a technique that enables the generation of few-cycle light pulses with energies in the millijoule range. The technique is based on propagation of laser pulses in a hollow fiber filled with noble gases (hollow fiber compression technique), see Figure 3.25.The modes of the hollow fiber are leaky modes, i.e. they experience radiation loss. However, there is one mode, the EH_{11}mode, which has considerably less loss than the higher order modes. This mode is used for pulse compression. The nonlinear index in the fiber can be controlled with the gas pressure. Typical fiber diameters are 100-500 μm and typical gas pressures are in the range of 0.1-3bar. As in the case of fiber compression it is important to consider the optimization of nonlinear interaction and dispersion. Both the medium and waveguide dispersion has to be taken into account. For more detail see ref. [107].

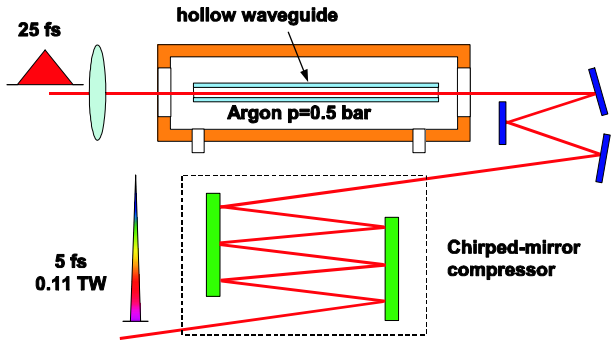

Figure 3.25: Hollow fiber compression technique [48]

For the time being, the hollow fiber compression technique is the only way to generate sub-10fs millijoule pulses. This will change soon with the advent of parametric chirped pulse amplification.

3.8 Appendix: Sech-Algebra

The hyperbolic secant is defined as

$$\mathrm{sech}(x) = \frac{1}{\cosh(x)} \tag{3.105}$$

See Figure 3.26

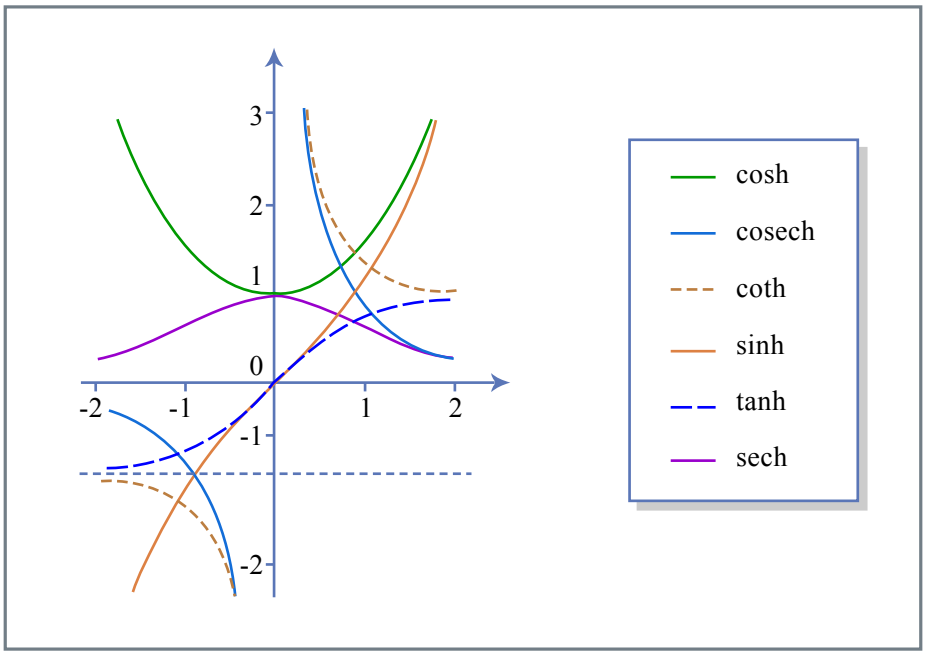

Figure 3.26: Hyperbolic functions

Figure by MIT OCW.

$$\cosh^2(x) - \sinh^2(x) = 1 \tag{3.106}$$

$$\mathrm{sech}^2(x) = 1 - \tanh^2(x) \tag{3.107}$$

$$\frac{d}{dx}\mathrm{sech}(x) = -\tanh(x)\mathrm{sech}(x) \tag{3.108}$$

$$\frac{d^2}{dx^2}\mathrm{sech}(x) = \mathrm{sech}(x)\left[1 - 2\mathrm{sech}^2(x)\right] \tag{3.109}$$

$$\int_{-\infty}^{+\infty} \mathrm{sech}(x)dx = \pi \tag{3.110}$$

$$\int_{-\infty}^{+\infty} \mathrm{sech}^2(x)dx = 2 \tag{3.111}$$

$$\int_{-\infty}^{+\infty} x^2\mathrm{sech}^2(x)dx = \frac{\pi^2}{6} \tag{3.112}$$

function $f(t)$	Fourier-Transform $\tilde{f}(\omega) = \int f(t)e^{-j\omega t}dt$
$\mathrm{sech}(t)$	$\pi\mathrm{sech}(\frac{\pi}{2}\omega)$
$\mathrm{sech}^2(t)$	$\frac{\pi\omega}{\sinh(\frac{\pi}{2}\omega)}$
$\mathrm{sech}^3(t)$	$\frac{1}{2}\left(1+\omega^2\right)\pi\mathrm{sech}(\frac{\pi}{2}\omega)$
$\mathrm{sech}^5(t)$	$\frac{1}{24}\left(\omega^4+10\omega^2+9\right)\pi\mathrm{sech}(\frac{\pi}{2}\omega)$
$\tanh(t)\mathrm{sech}(t)$	$-j\pi\omega\mathrm{sech}(\frac{\pi}{2}\omega)$
$\tanh^2(t)\mathrm{sech}(t)$	$\frac{1}{2}\left(1-\omega^2\right)\pi\mathrm{sech}(\frac{\pi}{2}\omega)$
$\tanh^3(t)\mathrm{sech}(t)$	$-j\frac{\omega}{6}\left(5-\omega^2\right)\pi\mathrm{sech}(\frac{\pi}{2}\omega)$
$\tanh(t)\mathrm{sech}^3(t)$	$-j\frac{\omega}{6}\left(1+\omega^2\right)\pi\mathrm{sech}(\frac{\pi}{2}\omega)$
$\tanh^2(t)\mathrm{sech}^3(t)$	$\frac{1}{2}\left(1+\omega^2\right)\pi\mathrm{sech}(\frac{\pi}{2}\omega) - \frac{1}{24}\left(\omega^4+10\omega^2+9\right)\pi\mathrm{sech}(\frac{\pi}{2}\omega)$
$t\tanh(t)\mathrm{sech}(t)$	$\pi\mathrm{sech}(\frac{\pi}{2}\omega) - \frac{\omega\pi^2}{2}\tanh(\frac{\pi}{2}\omega)\mathrm{sech}(\frac{\pi}{2}\omega)$
$t\tanh^2(t)\mathrm{sech}(t)$	$-j\omega\pi\mathrm{sech}(\frac{\pi}{2}\omega) - \frac{\pi^2}{4}\left(1-\omega^2\right)\tanh(\frac{\pi}{2}\omega)\mathrm{sech}(\frac{\pi}{2}\omega)$
$t\tanh^3(t)\mathrm{sech}(t)$	$\frac{1}{6}\left(5-3\omega^2\right)\pi\mathrm{sech}(\frac{\pi}{2}\omega) - \frac{\omega\pi^2}{12}\left(5-\omega^2\right)\tanh(\frac{\pi}{2}\omega)\mathrm{sech}(\frac{\pi}{2}\omega)$
$t\tanh(t)\mathrm{sech}^3(t)$	$\frac{1}{6}\left(1+3\omega^2\right)\pi\mathrm{sech}(\frac{\pi}{2}\omega) - \frac{\omega\pi^2}{12}\left(1+\omega^2\right)\tanh(\frac{\pi}{2}\omega)\mathrm{sech}(\frac{\pi}{2}\omega)$
$t\mathrm{sech}(t)$	$-j\frac{\pi^2}{6}\tanh(\frac{\pi}{2}\omega)\mathrm{sech}(\frac{\pi}{2}\omega)$
$t\mathrm{sech}^3(t)$	$-j\omega\pi\mathrm{sech}(\frac{\pi}{2}\omega) - j\frac{\pi^2}{4}\left(1+\omega^2\right)\tanh(\frac{\pi}{2}\omega)\mathrm{sech}(\frac{\pi}{2}\omega)$

3.9 Summary

We found, that the lowest order reversible linear effect, GVD, together with the lowest order reversible nonlinear effect in a homogeneous and isotropic medium, SPM, leads to the Nonlinear Schrödinger Equation for the envelope of the wave. This equation describes a Hamiltonian system. The equation is integrable, i.e., it does possess an infinite number of conserved quantities. The equation has soliton solutions, which show complicated but persistent oscillatory behavior. Especially, the fundamental soliton, a sech-shaped pulse, shows no dispersion which makes them ideal for long distance optical communication. Due to the universality of the NSE, this dynamics is also extremely important for modelocked lasers once the pulses become so short that the

spectra experience the dispersion and the peak powers are high enough that nonlinear effects become important. In general, this is the case for sub-picosecond pulses. Further, we found a perturbation theory, which enables us to decompose a solution of the NSE close to a fundamental soliton as a fundamental soliton and continuum radiation. We showed that periodic perturbations of the soliton may lead to side-band generation, if the nonlinear phase shift of the soliton within a period of the perturbation becomes comparable to $\pi/4$. Soliton perturbation theory will also give the frame work for studying noise in mode-locked lasers later.

A medium with positive dispersion and self-phase modulation with the same sign can be used for pulse compression. The major problem in pulse compression is to find a compressor that can that exactly inverts the group delay caused by spectral broadening. Depending on bandwith this can be achieved by grating, prism, chirped mirrors, puls shapers, AOPDFs or a combination thereof.

Bibliography

[1] L. Allen and J. H. Eberly: Optical Resonance and Two-Level Atoms, Dover (1987).

[2] A. Yariv, "Quantum Electronics", Wiley Interscience (1975).

[3] A. Hasegawa and F. Tapert, "Transmission of stationary nonlinear optical pulses in dispersive dielectric fibers. I. Anomalous dispersion," Appl. Phys. Lett. **23**, pp. 142 - 144 (1973).

[4] V. E. Zakharov and A. B. Shabat, "Exact Theory of Two-Dimensional Self-Focusing and One-Dimensional Self-Modulation of Waves in nonlinear Media", Zh. Eksp. Teor. Fiz. **34**, pp. 61 - 68 (1971); [Sov. Phys. - JETP **34**, pp. 62 - 69 (1972).]

[5] P. G. Drazin, and R. S. Johnson, "Solitons: An Introduction,"Cambridge University Press, New York (1990).

[6] G. B. Witham, "Linear and Nonlinear Waves," in Pure & Applied Mathematics Series, New York: Wiley-Interscience (1974).

[7] G. L. Lamb, Jr., "Elements of Soliton Theory," New York: Wiley-Interscience (1980).

[8] F. Schwabl, "Quantenmechnik," Springer, Berlin (1988).

[9] L. F. Mollenauer and R. H. Stolen, "The soliton laser" Opt. Lett. **9**, pp. 13 – 15 (1984).

[10] J. D. Moores, K. Bergman, H. A. Haus and E. P. Ippen, "Optical switching using fiber ring reflectors," J. Opt. Soc. Am. B **8**, pp. 594 – 601 (1990).

[11] L. F. Mollenauer, R. H. Stolen and J. P. Gordon, "Experimental observation of picosecond pulse narrowing and solitons in optical fibers", Phys. Rev. Lett. **45**, pp. 1095 – 1098 (1980).

[12] H. A. Haus and M. N. Islam, "Theory of the soliton laser," IEEE J. Quant. Electron. **QE-21**, pp. 1172 – 88 (1985).

[13] N. J. Zabusky and M. D. Kruskal, "Interactions of 'solitons' in a collisionless plasma and the recurrence of initial states," Phys. Rev. Lett., **15**, pp. 240 – 243 (1965).

[14] C. S. Gardener, J. M. Greene, M. D. Kruskal and R. M. Miura, "Method for solving the Korteweg-de Vries equation," Phys. Rev. Lett. **19**, pp. 1095 – 1097 (1967).

[15] M. J. Ablowitz, D. J. Kaup, A. C. Newell & H. Segur, "The inverse scattering transform - Fourier analysis for nonlinear problems," Stud. Appl. Math. **53**, pp. 249 – 315 (1974).

[16] A. C. Newell, "The Inverse Scattering Transform," In Topics in current physics. Solitons. ed. by R. Bullogh & P. Caudrey, Berlin, Springer (1978).

[17] V. A. Marchenko, "On the reconstruction of the potential energy form phases of the scattered waves," Dokl. Akad. Nauk SSSR, **104** 695 – 698 (1955).

[18] H. A. Haus, "Optical Fiber Solitons, Their Properties and Uses," Proc. of the IEEE **81**, pp. 970 – 983 (1993).

[19] R. Y. Chiao, E. Garmire, and C. H. Townes, "Self-trapping of optical beams," Phys. Rev. Lett. **13**, pp. 479 – 482 (1964).

[20] A. S. Davydov, "Solitons in molecular systems", Physica Scripta **20**, pp. 387 – 394 (1979). London: John Murray.

[21] Y. Kodama, and A. Hasegawa, "Nonlinear Pulse Propagation in a Monomode Dielectric Guide," IEEE J. Quantum Electron. **QE-23** pp. 510 – 524 (1987).

[22] A. Hasegawa, "Optical Solitons in Fibers," Springer Verlag, Berlin (1989).

[23] G. Placek, Marx Handbuch der Radiologie, ed. by E. Marx (Academische Verlagsgesellschaft, Leipzig, Germany, 1934), 2nd ed., Vol. VI, Part II, p. 209 – 374.

[24] F. X. Kärtner, D. Dougherty, H. A. Haus, and E. P. Ippen, "Raman Noise and Soliton Squeezing," J. Opt. Soc. Am. B **11** , pp. 1267 – 1276, (1994).

[25] V. I. Karpman, and E. M. Maslov, "Perturbation Theory for Solitons," Sov. Phys. JETP **46** pp. 281 – 291 (1977); J. P. Keener and D. W. McLaughlin, "Solitons under Perturbations," Phys. Rev. A **16**, pp. 777 – 790 (1977).

[26] D. J. Kaup, and A. C. Newell, "Solitons as particles, oscillators, and in slowly changing media: a singular perturbation theory," Proc. R. Soc. Lond. A. **361**, pp. 413 – 446 (1978).

[27] H. A. Haus and Y. Lai, "Quantum theory of soliton squeezing: a linearized approach," Opt. Soc. Am B **7**, 386 – 392 (1990).

[28] D. J. Kaup, "Perturbation theory for solitons in optical fibers", Phys. Rev. **A 42**, pp. 5689 – 5694 (1990).

[29] J. P. Gordon and H. A. Haus, "Random walk of coherently amplified solitons in optical fiber transmission," Opt. Lett. **11,** 665 – 668.(1986) .

[30] S. M. J. Kelly, "Characteristic sideband instability of periodically amplified average solitons", Electronics Letters, **28**, pp. 806 - 807 (1992).

[31] J. N. Elgin and S. M. J. Kelly, "Spectral modulation and the growth of resonant modes associated with periodically amplified solitons", Opt. Lett., **21**, pp. 787 - 789 (1993).

[32] J. Satsuma, and N. Yajima, "Initial Value Problems of One-Dimensional Self-Modulation of Nonlinear Waves in DIspersive Media," Supplement of the Progress in Theoretical Physics, **55**, pp. 284 – 306 (1974).

[33] J. P. Gordon, "Dispersive perturbations of solitons of the nonlinear Schrödinger equation", J. Opt. Soc. Am. B **9**, pp. 91 – 97 (1992).

[34] F. M. Mitschke and L. F. Mollenauer, "Discovery of the soliton self-frequency shift", Opt. Lett. **11**, pp. 659 – 661 (1986).

[35] J. P. Gordon, "Theory of the soliton self-frequency shift", Opt. Lett. **11**, pp. 662 – 664 (1986).

[36] A. C. Newell and J. V. Moloney, "Nonlinear Optics," Addison-Wesley Publishing Company, Redwood City, (1993).

[37] A.M. Kowalewicz, A. T. Zare, F. X. Kärtner, J. G. Fujimoto, S. Dewald, U. Morgner, V. Scheuer, and G. Angelow, "Generation of 150-nJ pulses from a multiple-pass cavity Kerr-lens modelocked Ti:Al2O3 oscillator," Opt. Lett., **28**, 1507-09, 2003.

[38] F. Gires, P. Tournois, C.R. Acad. Sci. (Paris) **258** 6112 (1964)

[39] J.A. Giordmaine, M.A. Duguaym J.W. Hansen: Compression of optical pulse, IEEE J. Quantum Electron. **4** 252-255 (1968)

[40] R. A. Fisher, P. L. Kelly, T. K. Gustafson: Subpicosecond pulse generation using the optical Kerr effect, Appl. Phys. Lett. **14** 140-143 (1969)

[41] A. Laubereau: External frequency modulation and compression of picosecond pulses, Phys. Lett. **29A** 539-540 (1969)

[42] H. Nakatsuka, D. Grischkowsky, A. C. Balant: Nonlinear picosecond-pulse propagation through optical fibers with positive group velocity dispersion, Phys. Rev. Lett. **47** 910-913 (1981)

[43] A.J. Campillo, S.L. Shapiro, B.R. Suydam: Periodic breakup of optical beams due to self-focusing, Appl. Phys. Lett. **23** 628-630 (1973)

[44] E.P. Ippen, C.V. Shank, T.K. Gustafson: Self-phase modulation of picosecond pulses in optical fibers, Appl. Phys. Lett. **24** 190-192 (1974)

[45] R.H. Stolen, C. Lin: Self-phase-modulation in silica optical fibers, Phys. Rev. A **17** 1448-1453 (1978)

[46] R.L. Fork, C.H.B. Cruz, P.C. Becker, C.V. Shank: Compression of optical pulses to six femtoseconds by using cubic phase compensation, Opt. Lett. **12** 483-485 (1987)

[47] A. Baltuška, Z. Wei, M.S. Pshenichnikov, D.A. Wiersma, R. Szipöcs: Optical pulse compression to 5 fs at a 1-MHz repetition rate, Opt. Lett. **22**, 102-104 (1997)

[48] M. Nisoli, S. De Silvestri, O. Svelto: Generation of high energy 10 fs pulses by a new pulse compression technique, Appl. Phys. Lett. **68** 2793-2795 (1996)

[49] M. Nisoli, S. De Silvestri, O. Svelto, R. Szipöcs, K. Ferencz, Ch. Spielmann, S. Sartania, F. Krausz: Compression of high-energy laser pulses below 5 fs, Opt. Lett. **22** 522-524 (1997)

[50] G. Cerullo, S. De Silvestri, M. Nisoli, S. Sartania, S. Stagira, O. Svelto: Few-optical-cycle laser pulses: from high peak power to frequency tunability, IEEE J. Selec. Topics in Quantum Electr. **6** 948-958 (2000)

[51] B. Schenkel, J. Biegert, U. Keller, C. Vozzi, M. Nisoli, G. Sansone, S. Stagira, S. De Silvestri, O. Svelto: Generation of 3.8-fs pulses from adaptive compression of a cascaded hollow fiber supercontinuum, Opt. Lett. **28** 1987-1989 (2003)

[52] G. P. Agrawal: *Nonlinear Fiber Optics* (Academic Press, San Diego 1995)

[53] *Ultrashort Laser Pulses,* Ed. W. Kaiser, Springer Verlag, 1988.

[54] A. Baltuška, Z. Wei, R. Szipöcs, M. S. Pshenichnikov, D. A. Wiersma: All solid-state cavity-dumped sub-5-fs laser, Appl. Phys. B **65** 175-188 (1997)

[55] E.B. Treacy: Compression of picosecond light pulses, Phys. Lett. **28A**, 34-35 (1968)

[56] R.L. Fork, O.E. Martinez, J.P. Gordon: Negative dispersion using pairs of prisms, Opt. Lett. **9** 150-152 (1984)

[57] R. Szipöcs, K. Ferencz, C. Spielmann, and F. Krausz, Opt. Lett. **19**, 201–203 (1994).

[58] R. Ell, U. Morgner, F.X. K\"{a}rtner, J.G. Fujimoto, E.P. Ippen, V. Scheuer, G. Angelow, T. Tschudi, Opt. Lett. **26**, 373-375 (2001)

[59] E.J. Mayer, J. Möbius, A. Euteneuer, W.W. Rühle, R. Szipöcs, Opt. Lett. **22**, 528 (1997).

[60] K. O. Hill, F. Bilodeau, B. Malo, T. Kitagawa, S. Theriault, D. C. Johnson, J. Albert, K. Takiguch, Opt. Lett. **19**, 1314-1316 (1994).

[61] A. V. Tikhonravov, M. K. Trubetskov, A. A. Tikhonravov, *OSA Topical Meeting on Optical Interference Coatings*, Tucson Arizona, February 7-12, 1998.

[62] B. Golubovic, R. R. Austin, M. K. Steiner-Shepard, M. K. Reed, S. A. Diddams, D. J. Jones and A. G. Van Engen, *Opt. Lett.* vol. 25, pp. 175-278, 2000.

[63] R. Scipöcs, G. DeBell, A. V. Tikhonravov, M. K. Trubetskov, Ultrafast Optics Conference, Ascona Switzerland, July 11-16, 1999.

[64] M. Matsuhara, K. O. Hill, Applied Optics **13**, 2886-2888 (1974).

[65] G. Tempea, V. Yakovlev, B. Bacovic, F. Krausz, and K. Ferencz, J. Opt. Soc. Am. B **18**, 1747-50 (2001).

[66] N. Matuschek, L. Gallmann, D. H. Sutter, G. Steinmeyer, and U. Keller, Appl. Phys. B **71**, 509-522 (2000).

[67] G. Steinmeyer, Conference on Lasers and Electro-Optics, Cleo 2003, Baltimore, June 2-6th, 2003.

[68] J. A. Dobrowolski, A. V. Tikhonravov, M. K. Trubetskov, B. T. Sullivan, and P. G. Verly, Appl. Opt. **35**, 644-658, (1996).

[69] A. Apolonski, A. Poppe, G. Tempea, C. Spielmann, T. Udem, R. Holzwarth, T. Hänsch, and F. Krausz, Phys.Rev.Lett. **85**, 740 (2000).

[70] R. Szipöcs and A. Kohazi-Kis, Applied Physics B **65**, 115-135 (1997).

[71] V. Laude and P. Tournois, paper CTuR4, Conference on Lasers and Electrooptics, Baltimore, USA, (1999).

[72] R. Szipöcs, A. Köházi-Kis, S. Lakó, P. Apai, A. P. Kovácz, G. DeBell, L. Mott, A. W. Louderback, A. V. Tikhonravov, M. K. Trubetskov, Applied Physics B **70**, S51-557 (2000).

[73] N. Matuschek, F.X. Kärtner, U. Keller, IEEE Journal of Quantum Electronics ,JQE- **5**, 129-137 (1999).

[74] V. Scheuer, M. Tilsch, and T. Tschudi, SPIE Conf. Proc.**2253**, 445-454,(1994).

[75] M. Tilsch, V. Scheuer, and T. Tschudi, SPIE Conf. Proc.**2253**, 414-422 (1994).

[76] F. X. Kärtner, U. Morgner, T. R. Schibli, E. P. Ippen J. G. Fujimoto, V. Scheuer, G. Angelow and T. Tschudi, J. of the Opt. Soc. of Am. **18**, 882-885 (2001).

[77] K. Naganuma, K. Mogi, H. Yamada, Opt. Lett. **15**, 393 (1990).

[78] I. Walmsley, L. Waxer, C. Dorrer: The role of dispersion in ultrafast optics, Rev. Scient. Instrum. **72** 1-29 (2001)

[79] J. Zhou, G. Taft, C.-P. Huang, M.M. Murnane, H.C. Kapteyn, I.P. Christov: Pulse evolution in a broad-bandwidth Ti:sapphire laser, Opt. Lett. **19** 1149-1151 (1994)

[80] R. Szipöcs, K. Ferencz, C. Spielmann, and F. Krausz: Chirped multilayer coatings for broadband dispersion control in femtosecond lasers, Opt. Lett. **19** 201-203 (1994)

[81] N. Matuschek, F. X. Kärtner, U. Keller: Theory of double-chirped mirrors, IEEE J. Select. Topics Quantum Electron. **4** 197-208 (1998)

[82] G. Tempea, F. Krausz, Ch. Spielmann, K. Ferencz: Dispersion control over 150 THz with chirped dielectric mirrors, IEEE J. Select. Topics Quantum Electron. **4** 193-196 (1998)

[83] F.X. Kärtner, N. Matuschek, T. Schibli, U. Keller, H.A. Haus, C. Heine, R. Morf, V. Scheuer, M. Tilsch, T. Tschudi: Design and fabrication of double-chirped mirrors, Opt. Lett. **22** 831-833 (1997)

[84] A.M. Weiner, D.E. Leaird, J.S. Patel, J.R. Wullert: Programmable femtosecond pulse shaping by use of a multielement liquid-crystal phase modulator, Opt. Lett. **15** 326-328 (1990)

[85] D. Yelin, D. Meshulach, Y. Silberberg: Adaptive femtosecond pulse compression, Opt. Lett. **22** 1793-1795 (1997)

[86] N. Karasawa, L. Li, A. Suguro, H. Shigekawa, R. Morita, M. Yamashita: Optical pulse compression to 5.0 fs by use of only a spatial light modulator for phase compensation, J. Opt. Soc. Am. B **18** 1742-1746 (2001)

[87] C. Iaconis, I.A. Walmsley: Self-referencing spectral interferometry for measuring ultrashort optical pulses, IEEE J. Quantum Electron. **35** 501-509 (1999)

[88] A.M. Weiner: Femtosecond pulse shaping using spatial light modulators, Rev. Scient. Instrum. **71** 1929-1960 (2000)

[89] C. Dorrer, F. Salin, F. Verluise, J.P. Huignard: Programmable phase control of femtosecond pulses by use of a nonpixelated spatial light modulator, Opt. Lett. **23** 709-711 (1998)

[90] M.A. Dugan, J.X. Tull, W.S. Warren: High-resolution acousto-optic shaping of unamplified and amplified femtosecond laser pulses, J. Opt. Soc. Am. B **14** 2348-2358 (1997)

[91] P. Tournois: Acousto-optic programmable dispersive filter for adaptive compensation of group delay time dispersion in laser systems, Optics Comm. **140** 245-249 (1997)

[92] F. Verluise, V. Laude, Z. Cheng, Ch. Spielmann, P. Tournois: Amplitude and phase control of ultrashort pulses by use of an acousto-optic programmable dispersive filter: pulse compression and shaping, Opt. Lett. **25** 575-577 (2000)

[93] J.P. Heritage, E.W. Chase, R.N. Thurston, M. Stern: A simple femtosecond optical third-order disperser, in Conference on Lasers and Electro-Optics, Vol. 10 of 1991 OSA Technical Digest Series (Optical Society of America, Washington, D.C., 1991), paper CTuB3.

[94] E. Zeek, K. Maginnis, S. Backus, U. Russek, M.M. Murnane, G. Mourou, H. Kapteyn, G. Vdovin: Pulse compression by use of deformable mirrors, Opt. Lett. **24** 493-495 (2000)

[95] A. Baltuška, T. Fuji, T. Kobayashi: Visible pulse compression to 4 fs by optical parametric amplification and programmable dispersion control, Opt. Lett. **27** 306-308 (2002)

[96] E.A.J. Marcatili, R.A. Schmeltzer: Hollow metallic and dielectric waveguide for long distance optical transmission and laser, Bell Syst. Tech. J. **43** 1783-1809 (1964)

[97] E.-G. Neumann: *Single-Mode Fibers* (Springer-Verlag, Berlin 1988)

[98] M. Nisoli, S. Stagira, S. De Silvestri, O. Svelto, S. Sartania, Z. Cheng, M. Lenzner, Ch. Spielmann, F. Krausz: A novel high energy pulse compression system: generation of multigigawatt sub-5-fs pulses, Appl. Phys. B **65** 189-196 (1997)

[99] M. Nisoli, E. Priori, G. Sansone, S. Stagira, G. Cerullo, S. De Silvestri, C. Altucci, R. Bruzzese, C. de Lisio, P. Villoresi, L. Poletto, M. Pascolini, G. Tondello: High-Brightness High-Order Harmonic Generation by Truncated Bessel Beams in the Sub-10-fs Regime, Phys. Rev. Lett. **88** 33902-1-4 (2002)

[100] T. Brabec, F. Krausz: Nonlinear Optical Pulse Propagation in the Single-Cycle Regime, Phys. Rev. Lett. **78** 3282-3285 (1997)

[101] S. Stagira, E. Priori, G. Sansone, M. Nisoli, S. De Silvestri, Ch. Gadermaier: Nonlinear guided propagation of few-optical-cycle laser pulses with arbitrary polarization state, Phys. Rev. A (in press) (2002)

[102] H.J. Lehmeier, W. Leupacher, A. Penzkofer: Nonresonant third order hyperpolarizability of rare gases and N_2 determined by third order harmonic generation, Opt. Commun. **56** 67-72 (1985)

[103] A. Dalgarno, A. E. Kingston: The refractive indices and Verdet constants of the inert gases, Proc. R. Soc. London Ser. A **259** 424-429 (1966)

[104] R. W. Boyd, *Nonlinear Optics*, Academic Press, San Diego (1992)

[105]

[106] G. Tempea, T. Brabec: Theory of self-focusing in a hollow waveguide, Opt. Lett. **23**, 762-764 (1998)

[107] S. De Silvestri, M. Nisoli, G. Sansone, S. Stagira, and O. Svelto, "Few-Cycle Pulses by External Compression" in "Few-Cycle Pulse Generation and Its Applications, Ed. by F. X. Kaertner, Springer Verlag, 2004.

[108] T. Brabec, F. Krausz: Intense few-cycle laser fields: frontiers of nonlinear optics, Rev. Mod. Phys. **72** 545-591 (2000)

[109] D. E. Spence, P. N. Kean, W. Sibbett: 60-fsec pulse generation from a self-mode-locked Ti:sapphire laser, Opt. Lett. **16** 42-44 (1991)

[110] D. Strickland, G. Mourou: Compression of amplified chirped optical pulses, Opt. Commun. **56** 219-221 (1985)